7. Technical development

Stockholm Conference Proceedings 2017, R. Holmberg et al

Cut-off in surface delays due to flyrock

D.P. Blair
Blasting Geomechanics Pty Ltd

ABSTRACT: When flyrock is generated from surface-delayed blasts, landing fragments can cut uninitiated portions of the surface delay system. If such a cut occurs, then blastholes further along the delay chain will fail to initiate. The probability of such a cut-off depends not only on the geology (which also influences launch conditions of the flyrock) but also on surface slope, surface delay times, in-hole delay times and the extent, size and exposure of the surface initiation system. Monte Carlo models were developed to predict the influence of these variables, excluding geology. The models require, as input, a source of rock fragments (from each blasthole) with prescribed launch properties, each with prescribed scatter. It is shown that, in any practical sense, the chance of getting a cut-off due to flyrock from a blast pattern on sloping ground is relatively insensitive to the slope angle. The models also show that the probability of a surface cut-off decreases at least exponentially (but often more rapidly) with increasing in-hole delay. Thus even a relatively small in-hole delay can produce a significant reduction in the probability of surface cut-offs.

1 INTRODUCTION

A blast misfire can occur if an uninitiated surface delay system is cut by flyrock produced by earlier-firing blastholes. The mining industry generally employs two alternative solutions to this problem. Firstly, a sufficiently large delay time (typically 400 ms or larger) is used within each blasthole, so that most of the surface delays have initiated before each hole initiates; this reduces the probability of cut-off. Secondly, electronic delays are used in which each hole initiates at its specified in-hole delay time without requiring any surface delays; this eliminates the possibility of cut-off. However, electronic delays are costly, and are not used by many blasting operations, especially those having a large number of blastholes per blast (such as cap rock blasting and iron ore shots). In fact, some cap rock blasting operations can involve thousands of short-length holes per blast and such operations often strive for efficiency using a detonating cord initiation system in which there are only surface delays (such as MS connectors) and no in-hole delays.

The probability that one or more rock fragments cuts an uninitiated surface delay is obviously related to the total number of airborne fragments produced by any blast. Clearly, it is impossible determine this number in any practical sense. However, in the present investigation, trajectories of a sufficiently large number of flyrock fragments can be simulated and cut-off

probabilities can then be estimated relative to the number of fragments. The main aim of the present investigation is to estimate the relative probability of surface cut-offs due to various delay sequences for various blast patterns fired on level or sloping ground. Section 2 deals with the analytical and numerical solutions describing flyrock motion; these solutions are required in order to determine the landing coordinates of the simulated flyrock. Section 3 deals with estimating the relative probability of a surface cut-off, which is expressed as the percentage concentration of critical flyrock landing over the blast pattern. In Section 4 these solutions and techniques are applied to estimate the relative probability of surface cut-off due to level and sloping ground as well as the influence of in-hole delay times on the probability of getting a surface cut-off.

2 FLYROCK MOTION INCLUDING AIR RESISTANCE (DRAG)

2.1 Drag forces

All bodies moving with a velocity V through a physical medium experience a drag force. A sufficiently general equation describing this drag force, D, can be given as:

$$D = bV + cV^2 \qquad (1)$$

where b is a constant describing linear drag and c a constant describing quadratic drag. Linear drag forces typically dominate for low-density bodies and/or motion in a sufficiently viscous medium (such as very small raindrops in air). Interestingly, for a large raindrop in air, both terms in Equation (1) must be used. Quadratic drag forces typically dominate for dense objects and/or motion in low viscosity media (such a flyrock in air). This is quite unfortunate for the present investigation because an exact analytical solution can only be obtained for the linear drag case. The quadratic drag case must be solved using a numerical solution. Nevertheless, important insights to flyrock behaviour can be obtained by considering the analytical solution under linear drag. Furthermore, the analytical solution can predict the landing coordinates from a few simple equations and so is typically 50 times faster to evaluate than the numerical solution, which requires 'time-stepping' over each trajectory path until impact occurs. It is also worthwhile noting that Chudinov (2002) gives an approximate analytical solution for the case of quadratic drag forces. However, this method will not be described here because its solution is rather lengthy and it is not simple to adapt for flyrock trajectories over sloping ground.

2.2 Launch geometry of fragments over sloping ground

Both the numerical and analytical models to be considered assume that each blasthole in an extended pattern produces N flyrock fragments, each having a particular mass m, launch velocity V_0, launch angle θ, and bearing (azimuth) angle ϕ defined positive in an anticlockwise direction from East. The relevant geometry for up-hill and down-hill flyrock trajectories is shown in Figure 1 for a ground surface sloping in the x-z plane only, and with a slope angle of α. The flyrock source for all particles from each blasthole originates at the point (x_0, y_0, z_0) in the local reference frame.

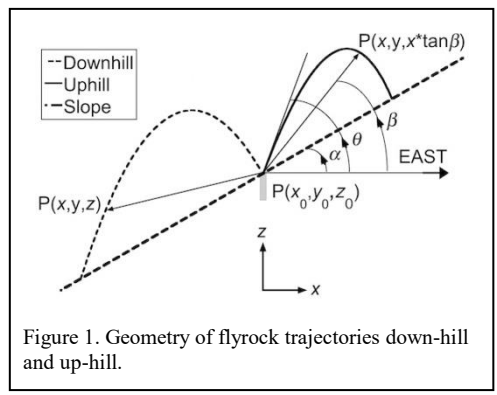

Figure 1. Geometry of flyrock trajectories down-hill and up-hill.

The three-dimensional launch velocity components are given by:

$$V_x = V_0 \cos\theta\cos\phi;\ V_y = V_0 \cos\theta\sin\phi;\ V_z = V_0 \sin\theta \qquad (2)$$

Ranges of the trajectory angles for a horizontal ground surface (α=0) are given by $0 \le \theta \le \pi/2$ and $0 \le \phi \le 2\pi$. However, for sloping ground the launch angles for up-hill fragments are restricted by the sloping surface and for down-hill fragments the launch angles can cover a much wider range. According to the convention shown in Figure 1, fragments travelling up-hill occur when $\cos\phi$ and α have the same sign, and fragments travelling downhill occur when $\cos\phi$ and $\tan\alpha$ have opposite signs. The lower range of allowable launch angles, θ, is then given by:

$$\tan\theta > \tan\alpha\cos\phi \quad (3)$$

2.3 Monte Carlo simulations for flyrock

The Monte Carlo component of the analytical and numerical models involves N simulations of flyrock launch conditions for each blasthole in a given blast pattern. For each simulation, ϕ is uniformly distributed between 0 and 2π and specified as $2\pi sr[0,1]$, where $sr[0,1]$ is a Sobol sub-random number between 0 and 1. These low discrepancy numbers span the space more evenly than the standard [0,1] pseudo-random numbers, and thus give faster convergence with increasing simulation number, N. The launch angle, θ, over horizontal ground is specified as a uniform distribution given by $sr[0,1]\pi/2$. However, in accordance with equation (3), for launch angles symmetrical about a vertical axis on a sloping ground, the launch angles are given by $\arctan(\tan\alpha\cos\phi)+sr[0,1]\{\pi/2-\arctan(\tan\alpha\cos\phi)\}$.

A uniform distribution of launch velocities is assumed between a maximum value (*VMAX*) and minimum value (*VMIN*) and thus the random launch velocities are defined by $V=VMIN + sr[0,1](VMAX-VMIN)$. The fragment masses, m, are generated as a non-uniform distribution based on a normal random number, derived from $sr[0,1]$, having a prescribed mean and standard deviation. Thus for each simulation, 4 independent sub-random numbers are required (one for each of ϕ, θ, V, and m) and these are generated using the 6-dimensional Sobol algorithm given in Press *et al.* (1992). The Monte Carlo programme also caters for a non-uniform distribution of launch angles and velocities (based on a mean and standard deviation). However, in the present investigation, all azimuth angles, launch angles and launch velocities are assumed to have a uniform distribution; only the fragment masses are given a non-uniform distribution.

2.4 Analytical model – linear drag

Assuming a horizontal ground surface, Fitzpatrick (2011) gives the equations describing projectile motion with air resistance (drag force) proportional to the velocity. In this case the vertical distance, $z(t)$, as a function of time, t, for a particle with a known terminal velocity, V_T, is given by:

$$z(t)=\frac{V_T}{g}\left(V_0\sin\theta+V_T\right)\left(1-\exp\left\{\frac{-gt}{V_T}\right\}\right)-V_T \quad (4)$$

where g is the acceleration due to gravity. The drag force, D, acting on a particle with 'frontal area', (i.e. cross section) A and density ρ, is given by:

$$D=A\rho C_D V^2/2 \quad (5)$$

where C_D is the drag coefficient (which is 0.45 for a rough sphere). In this regard, it should be noted that although the equation of motion (4) is only valid for a drag force proportional to V, the terminal velocity, itself, is calculated using the quadratic drag force equation given by (5). Although this could be viewed as some inconsistency with the model, it is worthwhile proceeding under this limitation. Terminal velocity is achieved when the drag force, D, acting on a particle of mass m, is equal to the gravitational force, mg. Thus, from (5):

$$V_T=\sqrt{\frac{2mg}{A\rho C_D}} \quad (6)$$

Assuming a rough spherical rock of diameter 0.1 m, equation (6) predicts a terminal velocity of 2.9 m/s (=104 km/h). The horizontal distance, $r(t)$, travelled by the particle is given by:

$$r(t)=\frac{V_0V_T\cos\theta}{g}\left(1-\exp\left\{\frac{-gt}{V_T}\right\}\right) \quad (7)$$

The x- and y-components of this horizontal distance are given by:

$$x(t)=r(t)\cos\phi;\ y(t)=r(t)\sin\phi \quad (8)$$

The range, R, of the flyrock is given as the horizontal distance to impact, i.e. the value of $r(t)$ when $z(t) = 0$ for $t > 0$. Thus, from (4) the time taken to land, t_R, is given by the solution to:

$$\frac{1}{g}\left(V_0\sin\theta+V_T\right)\left(1-\exp\left\{\frac{-gt_R}{V_T}\right\}\right)-t_R=0 \quad (9)$$

Once t_R is determined, the range, R, is then given from (7) as:

$$R=\frac{V_0V_T\cos\theta}{g}\left(1-\exp\left\{\frac{-gt_R}{V_T}\right\}\right) \quad (10)$$

However, in the present investigation, the ground is assumed to have a slope given by the angle α (Figure 1), and this replaces the impact condition

$z(t) = 0$ for horizontal ground by ($z(t)$ - $x(t)\tan\alpha$) = 0 for sloping ground. In this case (8) yields the impact condition:

$$z(t) - r(t)\cos\phi\tan\alpha = 0 \text{ at } t = t_R \tag{11}$$

Inserting (4) and (7) into (11) yields the solution to t_R for sloping ground as:

$$\frac{1}{g}\left(1-\exp\left\{\frac{-gt_R}{V_T}\right\}\right)\left(V_0\sin\theta + V_T - V_0\cos\theta\cos\phi\tan\alpha\right) - t_R = 0 \tag{12}$$

Equation (12) can be solved for t_R using Brent's method (Press et al. 1992) because all other parameters are known. The range of the landed flyrock is then given by (10), and its coordinates are given by:

$$x_L = R\cos\phi;\ y_L = R\sin\phi;\ z_L = R\cos\phi\tan\alpha \tag{13}$$

It should be appreciated that the launch angle, θ, in (12) is subject to the condition specified by (3). So far the solution has assumed that the blasthole radiates flyrock symmetrically about a vertical axis (to give some consistency with a vertical blasthole); this is defined as Condition 1 (see Figure 3, later). This symmetry condition is reasonable for flat, horizontal ground. However, this symmetry no longer holds for sloping ground, simply because there is less average burden on the down-slope side as 'seen' by any vertical blasthole, and a larger average burden 'seen' on the up-hill side. Thus it is also reasonable to investigate a model that assumes the flyrock to be radiated symmetrically about an axis normal to the slope; this is defined as Condition 2 (Figure 3). In reality, a combination of both these radiation mechanisms might be involved for sloping ground. Under Condition 2, the standard rotation matrix can be used to generate the flyrock components with respect to a rotation in the *x*-*z* plane only. Unfortunately, the analytical range Equations (7) and (10) are based only on a launch angle θ and not on an azimuth angle ϕ. Thus, for direct use in such equations, it is more convenient to derive new launch angles θ_n, and new azimuth angles, ϕ_n, consistent with a rotation of α in the *x*-*z* plane. Letting upper dashes signify the velocity components in the rotated system, then, by analogy with (2):

$$\begin{aligned} V_x' &= V_x\cos\alpha - V_z\sin\alpha \equiv V_0\cos\theta_n\cos\phi_n \\ V_y' &= V_0\cos\theta\sin\phi \equiv V_0\cos\theta_n\sin\phi_n \\ V_z' &= V_x\sin\alpha + V_z\cos\alpha \equiv V_0\sin\theta_n \end{aligned} \tag{14}$$

Equations (2) and (14) yield the solution given by Equation (15), which shows the new launch and bearing angles for flyrock radiated symmetrically about an axis normal to the slope. If $\alpha = 0$, then Equation (15) predicts that $\theta_n = \theta$ and $\phi_n = \phi$ as expected.

$$\begin{aligned} \theta_n &= \sin^{-1}\left(\cos\theta\cos\phi\sin\alpha + \sin\theta\cos\alpha\right) \\ \phi_n &= \tan^{-1}\left(\frac{\cos\theta\sin\phi}{\cos\theta\cos\phi\cos\alpha - \sin\theta\sin\alpha}\right) \end{aligned} \tag{15}$$

Thus for flyrock radiation symmetric about an axis normal to the slope, the angles θ and ϕ must be replaced by θ_n and ϕ_n, respectively, in equations (11) to (13).

2.5 Numerical model – quadratic drag

Each fragment is generated at the source and tracked using a fourth-order Runge-Kutta method to integrate the equations of motion, step by step, under the influence of air drag given specifically by the quadratic drag Equation (5). This method requires a specified time interval, *dt*, for each step; too coarse a value of *dt* yields an inaccurate trajectory, too fine a value requires excessive computing time. Furthermore, after each step, the fragment coordinates are tested to see if an impact has occurred with the ground. Thus this step-by-step process, although robust, is time-consuming. In order to improve the trade-off between accuracy of landing coordinates and time step, *dt*, the coordinates of the prior point to landing ($x_{L\text{-}1}$, $y_{L\text{-}1}$, $z_{L\text{-}1}$) and the predicted landing point (x_L, y_L, z_L) were used to define a line in 3D space. The intersection of this line with the angled surface plane was then determined by standard 3D geometry. This intersection point is a more accurate estimation of the landing coordinate, and allows a coarser time step without severe penalty. One advantage of the numerical solution is that it deals directly with initial component values, and thus it is not required to derive equivalent launch and azimuth angles (as in 15). Hence for sloping ground all that is required at the start of each trajectory is to transform V_x and V_z in equation (2) using the standard rotation matrix; V_y is left unaltered.

3 CRITICAL FLYROCK FROM A SPATIAL DISTRIBUTION OF BLASTHOLES

The analytical and numerical models predict the landing coordinates (x_L, y_L, z_L) of each flyrock fragment and the time, t_R (according to equation

12, from each blasthole in a local reference frame. In this frame, the blasthole is located at (0, 0, 0) and initiated at zero time. If (x_{Bj}, y_{Bj}, z_{Bj}) are the true coordinates of the j th blasthole in a blast pattern and t_{Bj} is its initiation time, then the true coordinates of a landed flyrock fragment produced by this blasthole and the true time to landing are given by:

$$(x_{Tj}, y_{Tj}, z_{Tj}) = (x_{Bj} + x_L, y_{Bj} + y_L, z_{Bj} + z_L) \quad (16)$$
$$t_{Tj} = t_{Bj} + t_R$$

Rock fragments that have the potential to produce a surface cut-off must satisfy three requirements. Firstly, the fragments must land within the blast pattern; more specifically, they must lie within the concave hull of all the blastholes (see the discussion with regards to Figure 2 later). Secondly, the landing time of these particles must be less than the largest initiation time of all blastholes. Thirdly, fragments must also land on zones of the blast pattern containing uninitiated blastholes. Fragments that satisfy these conditions are called critical, and their landing coordinates are designated (x_C, y_C, z_C). A method to achieve the third requirement for each fragment is now presented. Any active (i.e. un-initiated) blasthole at the moment of fragment impact must have a delay time greater than t_{Tj} (of Equation 16), and the set of distances between the landed fragment in question and all such active blastholes is then determined. If the minimum distance, d_{M1}, of this set is less than the average blasthole spacing, then the fragment lies close to an uninitiated hole and so is considered to have the potential to produce a cut-off. However, a further test is required, because such a fragment could also be even closer to a previously initiated blasthole (i.e. a blasthole lying in sterile ground). Thus the set of distances between the landed fragment and all initiated blastholes is also determined, and the minimum distance, d_{M2}, of this set is then calculated. If $d_{M1} < d_{M2}$, then the particle is considered to be critical with regard to flyrock cut-off; under the present model, only such particles can cause a surface delay cut-off.

In the case of sloping ground, there are two alternatives. The first alternative is to preserve the blasthole coordinates (i.e. burden and spacing) in the horizontal plane; this implies an increase in pattern surface area for non-zero slope angles. The second alternative is to preserve the pattern surface area; this implies a reduction in the burden and/or spacing for non-zero slope angles. It was decided to present only those models that conserve the blasthole coordinates in the horizontal plane, as this is consistent typical drilling operations.

As noted in the Introduction, it is impossible to determine the number of flyrock fragments from any blasthole, and thus it is impossible to give any absolute determination of the probability of flyrock cut-off. However, it is possible to simulate a number of flyrock particles and determine the landing coordinates and the percentage, P_C, of such particles that become critical. This enables a determination of the percentage concentration of critical flyrock throughout the blast pattern of interest. Of course, it is also possible to include a refinement using the ratio R_C, of the exposed area of the surface initiation system to the total area of the blast pattern. This ratio will necessarily be very small and constant for a given surface delay system and blast pattern. The refined estimate of the relative probability of surface cut-off would then be given by $R_C P_C$. For example, if a representative region of the surface initiation can be classified by a spacing S (typically the blasthole spacing) between surface delay trunk lines each having a diameter d (typically 0.004 m for a detonating cord line) then the chance of a critical fragment of radius r (typically 0.1 m) hitting the delay line is approximately $R_C = (d+2r)/S$; inserting typical values yields $R_C = 0.03$. Based on this simple model there is a 3% chance, on average, that critical fragments will impact the surface trunk line and produce a cut-off. However, such a refined estimate will not be included; after all, P_C, itself, is still only a relative measure.

4 RESULTS

4.1 A cap-rock blast over horizontal and sloping ground

Figure 2 shows the spatial pattern of the 478-hole cap-rock blast overlaid on a map of the delay times, the blast duration is 7.58 s; the point of initiation is also shown. The thick white boundary surrounding the blastholes is the concave hull of all blastholes, which is derived from the convex hull using the ‘gift-opening’ algorithm of Rosen et al. (2014). This cap-rock blast used surface cord initiation with MS surface delays and no in-hole delays. Figure 3 shows the trajectories predicted by the Runge-Kutta (numerical) model for a sloping ground under Condition 1 (lower figure) for which the flyrock is symmetrical about a vertical axis, and Condition 2 (upper figure) for which the flyrock is symmetrical about an axis

normal to the sloping surface. The random suite of launch velocities, *V*, is identical in both cases. Clearly the flyrock trajectories will depend upon which type of launch condition is assumed; it is quite possible that in reality the flyrock for blastholes on sloping ground will involve an aspect of both conditions. All trajectories are seen to end precisely on the sloping surface as required, due to the 3D geometric interpolation previously mentioned.

Figure 4 shows an example using the numerical model with 100 fragment simulations from each blasthole fired on horizontal ground. The launch velocities, *V*, were distributed as 3+27**sr*[0,1] m/s (i.e. uniformly distributed over the range 3 m/s to 30 m/s), the launch angles, θ, and bearing angles, ϕ, were distributed as described in Section 2.3. All fragments lying outside the blast zone are shaded grey and all the critical fragments lying within the blast are black. Figure 4 shows a clear spatial variation in the density of critical fragments (for example there is a relatively low concentration in a region near the initiation point).

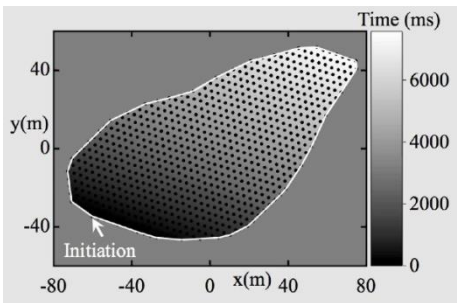

Figure 2. Spatial layout and delay time map for the cap-rock blast.

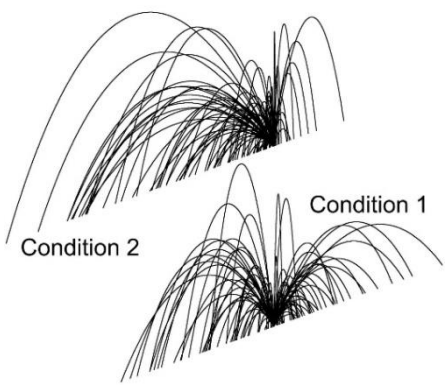

Figure 3. Flyrock generation on sloping ground.

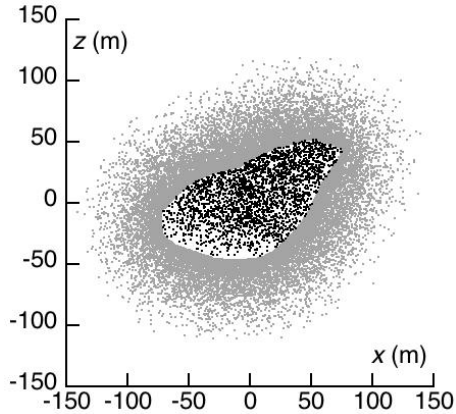

Figure 4. Landed fragments outside; critical fragments within.

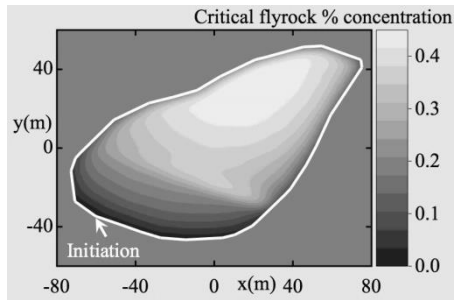

Figure 5a. Flyrock distribution; numerical model, $\alpha = -20^{O}$.

However, such variations are best quantified by using kernel density estimation. In the present work, a bivariate Gaussian kernel is used with an optimal, data dependent, bandwidth determined by Scott's Rule. Figures 5a, 5b and 5c show the percentage concentration of critical flyrock fragments (with respect to total flyrock fragments) obtained using 10,000 simulations for each blasthole in the model under consideration, but with slope angles, α, of -20, 0 and +20 degrees, respectively, and obeying the launch Condition 1 (Figure 3). Figures 5a, 5b and 5c show that if a surface cut-off does occur, then it will most likely be found in that region containing the highest concentration of critical flyrock (i.e. in the central northern region). It can be seen that changing the slope angle changes the surface distribution of critical flyrock as well as the percentage concentration levels. All figures are plotted on the same scale, and so it can be seen that the case for

α = -20 degrees has the largest zone of peak concentrations and the case for α = +20 has the smallest zone of peak concentrations.

Figure 6 shows the relationship between the ground slope and critical flyrock fragments. The flyrock parameter used is the ratio of the number of critical flyrock fragments to the total number of generated fragments. Obviously for a sufficient number of Monte Carlo simulations, *N*, this ratio will be independent of *N*. Figure 6 shows the results for both launch conditions (Figure 3) and both models (numerical and analytical). There are two main points of interest. Firstly, there is a notable, but not significant, difference between launch Condition 1 and 2. As noted previously, it seems reasonable to suspect that the more realistic case might be some combination of the two conditions. This would then imply that, in any practical sense, the probability of getting a cut-off due to flyrock is relatively insensitive to slope angle (note the limited range of the vertical axis). Secondly, the analytical model predicts fewer critical fragments when compared with the numerical model, and this is due to the less realistic drag forces implied by this model. Nevertheless, it is worthwhile noting the trend between the analytical and numerical models. In this regard the drag coefficient, C_D, for both models is assumed to be 0.45 (for rough spheres). However, when this coefficient was reduced to 0.1 in the analytical model, the resulting predictions for both launch conditions (not shown) were almost identical to those of the numerical model. This particular finding, under the present Monte Carlo flyrock simulations, suggests that the (fast) analytical model could be a useful tool for flyrock analysis. In this regard, the execution time for the numerical model with N = 10000 for all slopes considered (intervals of 1 degree) was 9.4 hours for each plot in Figure 6; the execution time using the analytical model was only 0.16 hours. Thus for this particular problem, the analytical model is approximately 60 times faster than the numerical model.

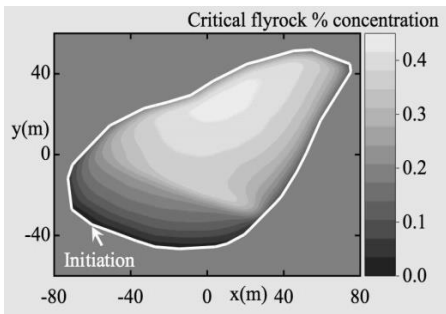

Figure 5b. Flyrock distribution; numerical model, α = 0.

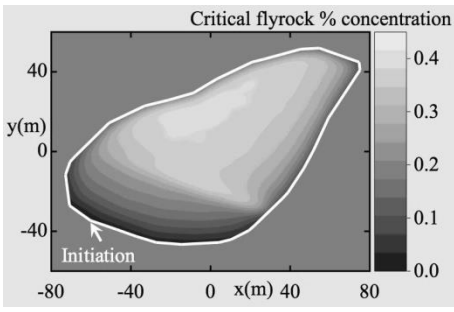

Figure 5c. Flyrock distribution; numerical model, α = +20^O.

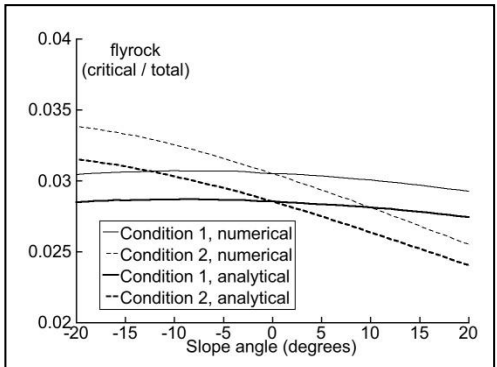

Figure 6. Model comparisons for sloping ground.

Figure 7 shows the critical flyrock concentration predicted by the analytical model for horizontal ground (α = 0) with the standard drag coefficient of 0.45. As expected, the peak level is lower than that predicted by the numerical model (as shown in Figure 5b); however there is a similarity in the relative distribution of the concentration throughout the blast pattern, again emphasising the value of the analytical model.

4.2 A large open pit blast

Figure 8 shows the spatial pattern of the 320-hole blast overlaid on a map of the surface delay times; the point of initiation is also shown; delay times start at 0.4 s due to the 400 ms in-hole delay. The

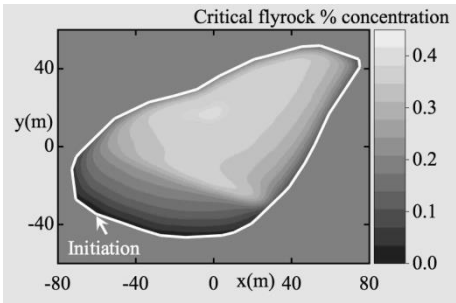

Figure 7. Flyrock distribution; analytical model, $\alpha = 0$.

thick white boundary is the concave hull of all blastholes. The maximum duration of this blast is 1.95 s, which is approximately 4 times smaller than the duration of the cap-rock blast (which, incidentally, had no in-hole delays – see Figure 2). As noted previously, the landing time of all critical fragments must be less than the blast duration, otherwise a cut-off cannot occur. Thus, irrespective of any in-hole delay, reducing the duration (as in the open pit blast) will reduce the number of critical fragments, especially since the lateral extents of both blasts are not completely dissimilar. Also, increasing the in-hole delay will further decrease the number of critical fragments because it artificially increases all fragment landing times by the in-hole time. Thus the selection of an appropriate in-hole delay has significant practical implications with regard to designing a blast that is not susceptible to surface delay cut-offs. This design aspect is now considered with regard to the open pit blast, and model results for horizontal ground ($\alpha = 0$), only are given. For this blast, the launch velocities, *V*, were distributed as 10+90**sr*[0,1] m/s (i.e. uniformly distributed over the range 10 m/s to 100 m/s), all other launch conditions were unchanged.

Figure 9a shows the critical flyrock concentration predicted by the numerical model assuming an in-hole delay of 0.0 s, and Figure 9b shows the predictions using the analytical model. As noted previously, the numerical model is far more numerically intensive than the analytical model. In the present case, the numerical model used 200,000 Monte Carlo simulations for each blasthole and required 10.5 hours execution time, whereas the analytical model used 1 million simulations and required 8 mins execution time. Thus for this particular model, the analytical model is 387 times faster than the numerical model.

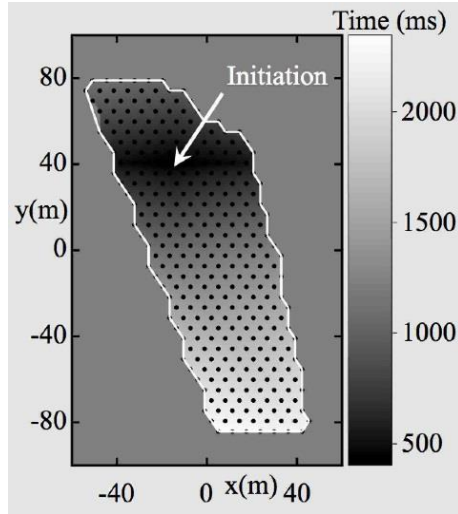

Figure 8. Spatial layout and delay time map for the open pit blast.

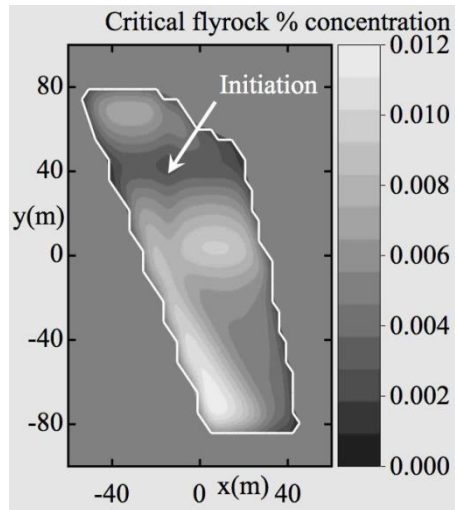

Figure 9a. Numerical model; zero in-hole delay.

Figures 9a and 9b show that the numerical and analytical models give very similar predictions. Figures 10a and 10b show the numerical and analytical predictions, respectively, assuming an in-hole delay of 0.1 s. It is clear from Figures 9 and 10 that even a small in-hole delay produces a significant reduction in the probability of a surface delay cut-off.

Figure 11 shows the results from the analytical model assuming an in-hole delay of 0.2 s and

Figure 12 shows the results assuming an in-hole delay of 0.4 s (as used for the actual blast). It is obvious that increasing the in-hole delay from 0.2 s to 0.4 s gives a significant reduction in the number of critical fragments (note scales on each plot) and also significantly reduces the area of concentration. Thus, for the actual blast, if a surface delay cut-off had been observed (in fact such was not the case) then the model predicts that there is a high likelihood that it would have occurred in the south-west extremity of the blast pattern.

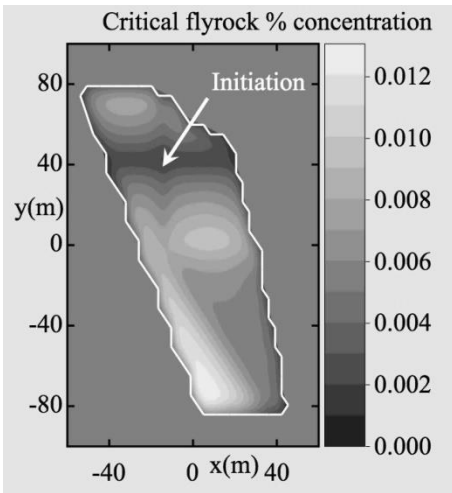

Figure 9b. Analytical model; zero in-hole delay.

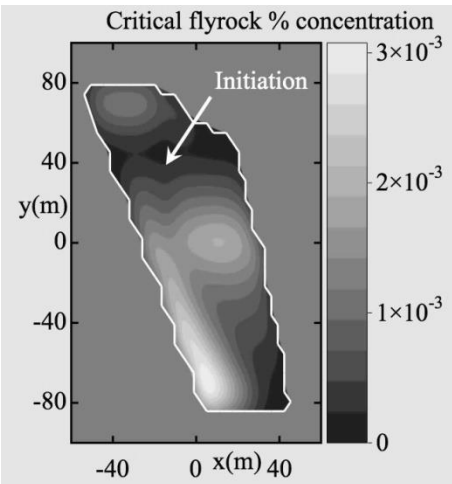

Figure 10a. Numerical model; in-hole delay 0.1 s.

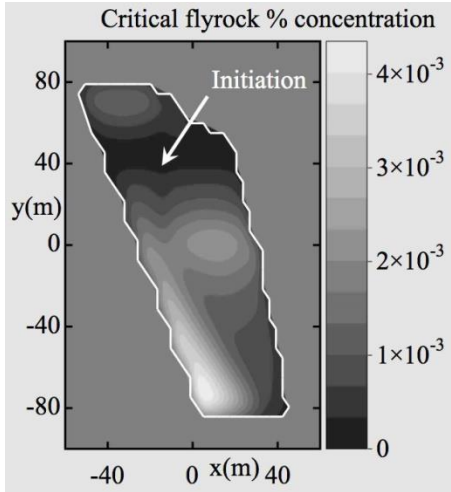

Figure 10b. Analytical model; in-hole delay 0.1 s.

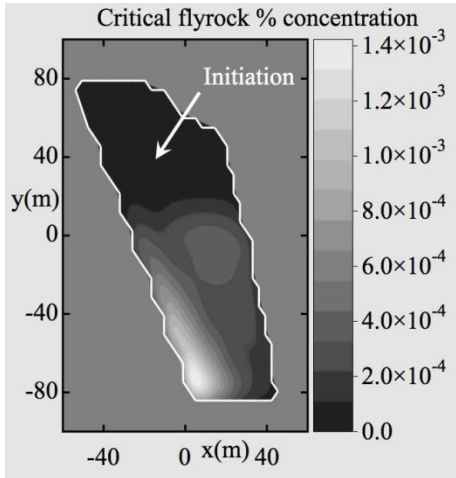

Figure 11. Analytical model; in-hole delay 0.2 s.

The analytical model was then used to determine the influence of a large range of in-hole delays; for each delay, a million simulations were used for each blasthole in the open pit blast pattern. Figure 13 shows the ratio of critical fragments to the total number of fragments as a function of the in-hole delay and for various values of the maximum launch velocity, *VMAX*. In this regard the launch velocities, *V*, were distributed as *VMIN* + *sr*[0,1](*VMAX*-*VMIN*) m/s; where *VMIN* was fixed at 0.3 m/s. The ratio is plotted on a log scale and shows that for *VMAX*=150 m/s, the number of critical fragments

decreases almost exponentially with in-hole delay. For lower values of *VMAX*, the number of such fragments decreases even more rapidly with in-hole delay. These results clearly show the effectiveness of increasing the in-hole delay to avoid surface cut-offs.

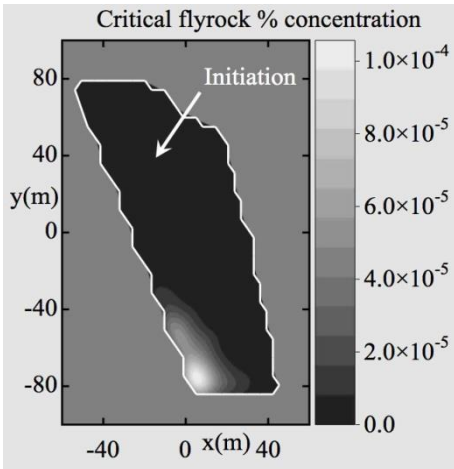

Figure 12. Analytical model; in-hole delay 0.4 s.

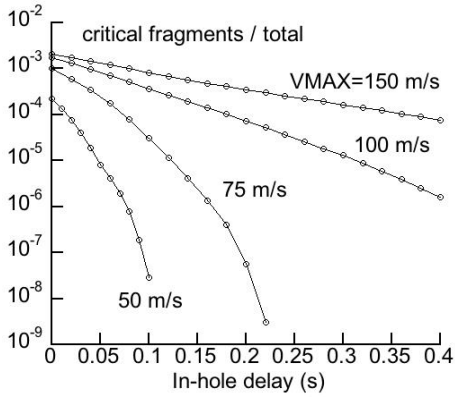

Figure 13. Critical flyrock as a function of in-hole delay.

5 CONCLUSIONS

A numerical model and an analytical model were used to predict the landing coordinates of critical flyrock fragments, i.e. those fragments that play a crucial role for impacting surface trunk lines and causing surface cut-offs. Two types of blasts were analysed: a cap rock blast and an open pit blast. The cap rock blast used no in-hole delays and was fired on sloping ground. Figure 5 shows that the distribution of critical flyrock over the blast pattern changes with slope angle. Figure 6 shows the ratio of the number of critical flyrock fragments to the total number for two conditions of flyrock launching (illustrated in Figure 3). As noted previously from an argument based on symmetry, it is possible to view the real situation as some combination of these two conditions for blasting on sloping ground. The results of Figure 6 also imply that, in any practical sense, the probability of getting a cut-off due to flyrock is relatively insensitive to slope angle.

The models for the open pit blast showed that using even a modest in-hole delay can give a significant reduction in the probability of getting a surface delay cut-off. If the typical in-hole delay (0.4 s) is used then the resulting probability is miniscule. Furthermore, increasing the in-hole delay severely restricts the region of the blast pattern most likely to give rise to any cut-off (see Figure 12). Figure 13 shows the effectiveness of increasing the in-hole delay to avoid flyrock fragments producing a cut-off in the surface delay sequence.

REFERENCES

Chudinov, P.S. 2002. Approximate analytical investigation of projectile motion in a medium with quadratic drag force. *Int. J. Sports Sci & Eng*., v5, 27-42.

Fitzpatrick, R. 2011. Newtonian Dynamics: Projectile motion with air resistance. University of Texas, p 47-51.

Press, W.H., Teukolsky, S.A., Vetterling, W.T. and Flannery, B.P. 1992. Numerical Recipes. *The Art of Scientific Computing, Second Edition*, Cambridge University Press, New York, 963 pp.

Rosen, E., Jannson, E. and Brundin, M. 2014. Implementation of a fast and efficient concave hull algorithm. *Project in Computational Science*, Dept. Info. Sci., University of Uppsala, pp34.

Stabilisation of emulsion explosives utilising optimised co-surfactant systems - increased efficiency

E. Kharatyan
AEL Mining Services, AECI Group, Johannesburg, South Africa

ABSTRACT: An emulsion explosive is a dispersion of two relatively immiscible liquids/phases: an aqueous oxidizer phase and a hydrocarbon fuel phase. A third component, named surfactant/emulsifier, is required to stabilise an emulsion by preventing phase separation. Emulsion explosives (EE) are commonly stabilised by poly (isobutylene) succinic anhydrite (PIBSA-based) surfactants in combination with sorbitan esters (SPAN). In such a system, the SPAN emulsifier stabilises the newly formed oxidizer/fuel surfaces during emulsion formation and pumping (shearing), whereas the PIBSA-based surfactant forms a structured bilayer or micelles in order to suppress emulsion phase separation. This system is however not always the most efficient as the choice of surfactants for EE co-surfactant system is usually a compromise that is based on the performance of individual surfactants, which does not consider the synergy of the surfactants in the system. Usually, only averaged emulsion explosives formulation is produced in order to cover (to a certain extent) all the customers' requirements. Therefore, it is always desirable to optimise the current co-surfactant system in order to improve the efficiency of the system and make it customer oriented (flexible). An optimised surfactant system is required to make this possible. As a result of these requirements, a number of new co-surfactant systems were researched and developed. For example, an optimised system allows for a reduction of the total active level in the emulsion explosives' fuel phase keeping the shelf-life stability of emulsion explosives the same. The other optimised co-surfactant system allows the use of lower grade fuels, where the content of recycled used oils in the emulsion explosives' fuel phase formulation can be increased and fully replace the clear diluent oils. In addition to the above based on the customer's demand the co-surfactants system can be optimised in a way to allow: the use of different grades of diesel; the improvement of the carbon footprint; the improvement of the emulsion explosives' stability on shelf and in pumping; the improvement of the emulsion explosives' sleep time in the blast-hole; the improvement of emulsion explosives' blast performance.

1 INTRODUCTION

Emulsion explosives (EE) are a special type of emulsion. As a common emulsion, EE is a colloidal mixture of two immiscible or partially immiscible liquids, usually referred to as water/oxidizer and oil/fuel phase. There is an additional component in the emulsion

composition. This component, which is called surfactant, serves to enable effective emulsion formation and shelf-life stability (Masalova *et al.* 2006 and 2007, Kim *et al.* 2008, Tshilumbu *et al.* 2010, Drelich *et al.* 2010). The role of the surfactant in a standard emulsion is to decrease the water-oil phase interfacial tension, to create a strong water-oil interface and to form a steric barrier in order to prevent emulsion from gravitational phase separation, creaming, coalescence, flocculation or Ostwald ripening (Becher 1985, Hunter 1986, Schramm 1992, Hunter 1993, McClements 1999). EE require a higher degree of stability (Masalova *et al.* 2006, Tshilumbu *et al.* 2010). Stability to crystallisation, different grades of fuel and raw materials must be considered. At the same time, while the shelf-life stability is improved, the emulsion pumpability, interfacial chemical reaction of sensitisation as well as ammonium nitrate porous prill compatibility should not be compromised. Conventionally, EE is stabilised by a system of two types of surfactants: sorbitan ester (SPAN) that provides stability in pumping, and poly(isobutylene) succinic anhydride based surfactant (PIBSA-based) to provide shelf-life stability. Such a surfactant system is not always the most efficient.

The current investigation concentrates on the optimisation of new co-surfactant systems in order to make such systems more efficient and flexible (customer oriented).

2 EXPERIMENTAL

2.1 Materials

Industrial grade fuels were used as supplied. Industrial grade emulsifiers were used as supplied. A desired amount of surfactants was dissolved in industrial fuel in order to prepare an EE continuous/fuel phase. Emulsion grade ammonium nitrate was used in order to produce the emulsion dispersed phase, which was a supersaturated water solution of ammonium nitrate. The above materials were used in order to manufacture highly concentrated emulsions where the continuous phase did not exceed 10% of the emulsion by mass. A more detailed description of the emulsions and emulsion preparation can be found elsewhere (Masalova *et al.* 2006, 2007).

2.2 Methods

A Hobart N50 mixer was used to manufacture all the samples under study. A more detailed description of emulsion manufacturing can be found elsewhere (Masalova *et al.* 2006 and 2007, Tschilumbu *et al.* 2010). The final viscosity of the respective emulsions was in the range of 18,000 to 22,000 cP (@70 ^{o}C), which was measured by means of a Brookfield viscometer at a rotational speed of 50 rpm (spindle No 7). The optical analyses were conducted by means of 'Leica' optical microscope equipped with a digital camera. The magnification was kept at 40x magnification. The structural changes of the materials with ageing were followed. The pumping was performed using the AEL Mining Services double syringe test at 4 bar pressure. The pumping was done through a 5 mm orifice. Few 'pumping cycles' were carried out. In order to accelerate the shelf-life stability test, closed containers filled with emulsion samples were placed in an oven at a temperature of 40 ^{o}C. The stability tests were followed by microscopy. Over gassing resistance of doped with Ammonium Nitrate Porous Prills (ANPP) sensitised emulsion explosives where the compatibility of the ANPP and the oil/surfactant in the emulsion were determined as well. The test was conducted at higher than ambient temperature (55 ^{o}C) with excess gasser. Velocity of detonation (VoD) of EE was determined for sensitised EE that was placed into plastic or cardboard pipes. All the pipes were transported to the test range and fired. The time taken for the shockwave to travel a distance of ~15 cm was measured using an AECE VD Timer (model VOD-3). The VoD was calculated based on the results of these measurements.

3 RESULTS AND DISCUSSIONS

EE are commonly stabilised by poly (isobutylene) succinic anhydride based surfactant (PIBSA-based) in combination with sorbitan ester (SPAN). In such a system each surfactant contributes towards certain emulsion properties. For example, the SPAN emulsifier stabilises the newly formed oxidizer/fuel interfaces enabling the emulsion formation, refinement and pumping stability, whereas the PIBSA-based surfactant forms a structured bilayer or micelles in order to supress phase separation. The system is not always the most efficient and has its limitations. It was mentioned before that EE stabilisation considers many parameters:

- EE formation
- EE refinement
- EE stability in pumping

- EE ability to be sensitised and ease of the sensitisation
- EE stability to crystallisation with time
- EE ammonium nitrate porous prill compatibility
- Sensitised and doped emulsion sleep time stability
- EE blast performance, etc.

One surfactant can only cover (to some extent) the improvement of one, two and sometimes three parameters. Often, when the surfactant improves certain parameters, it lowers the efficiency of the other surfactant at the same time. A common EE surfactants combination is the PIBSA-based / sorbitan monooleate (SMO) surfactant system. PIBSA-based surfactant performs well on its own improving EE stability to crystallisation, separation, but it gives the EE a low to no stability in pumping. The addition of SMO helps to solve the pumpability issue but reduces drastically the EE stability to crystallisation with ageing (Figure 1).

Therefore, the choice of surfactants for EE co-surfactant system is usually a compromise that is based on the performance of individual surfactants, which does not consider the synergy of the surfactants in the system. Averaged compromised emulsion explosives formulation is produced and supplied to the customers in order to cover (to a certain extent) requirements of all customers. There is a need for optimised co-surfactant systems that will take into account the performance of individual surfactants as well as the synergy of these surfactants. This allows improving the efficiency of surfactants based on stronger Surfactant X – Surfactant Z – Surfactant Y bonding in comparison to Surfactant X – Surfactant Y bonding, resulting in a stronger interface and micelles (Figure 2). The improved efficiency of a certain surfactant effect by addition of co-surfactant based enhancer will allow adjusting the EE formulation in terms of co-surfactants combination based on the customer requirement supplying the flexibility and better services to the customer.

The utilisation of such optimised systems can improve the shelf-life stability of EE. The stability of emulsions was investigated in terms of the dispersed phase droplet crystallisation. The

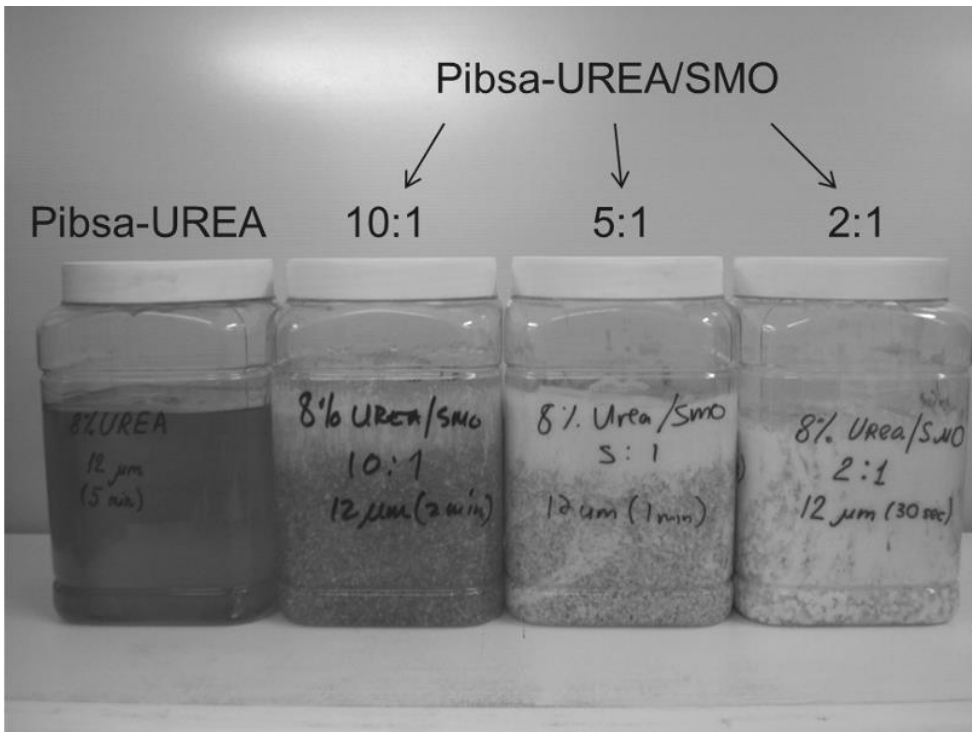

Figure 1. Effect of SMO addition to PIBSA-based surfactant on EE stability to crystallisation.

crystals can be observed in the polarised microscopy as white spots on a black background. As can be seen from the Table 1 the EE stabilised with an optimised surfactant system is more stable than the EE stabilised with a conventional surfactant system. Since the stability of EE stabilised by conventional surfactant system is acceptable, the amount of total surfactants in the optimised system can be reduced in order to achieve a similar stability to the conventional system (Figure 3 and Table 2).

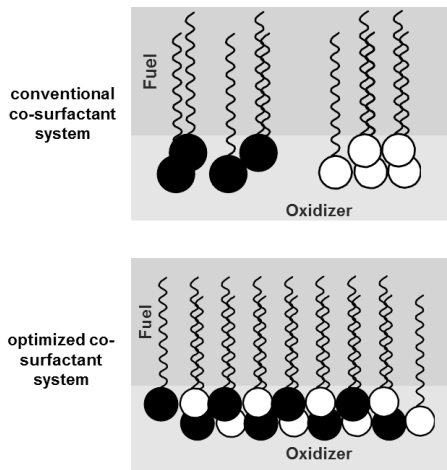

Figure 2. Schematic representation of common and optimised co-surfactants system.

Table 1. Polarised microscopy images of aged for 48 days EE: (a) manufactured and un-pumped EE; (b) manufactured and pumped emulsion. Magnification 40x.

EE stabilised by conventional surfactant system	*EE stabilised by optimised surfactant system*
(a)Un-pumped	
(b)Pumped	

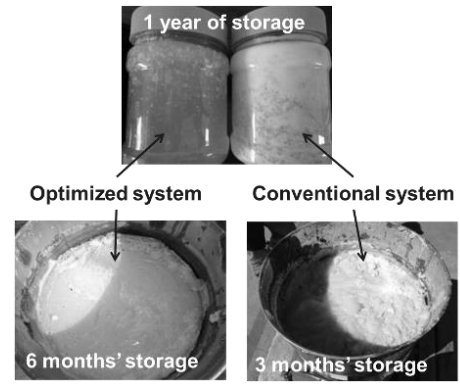

Figure 3. Comparison of EE stability to ageing for different optimised surfactant systems - lowered total surfactants in optimised system of co-surfactants.

Table 2. Comparison of EE stability to ageing for different optimised surfactant systems – substantial reduction of total surfactants. Magnification 40x.

Ageing	6 Weeks
Conventional surfactant system	
Optimised surfactant system	

Different optimised systems were tested with different EE products. It was shown that among improved stability to ageing, other EE properties were improved when the system of co-surfactants was optimised. Such optimised co-surfactant systems can accommodate oils, such as reworked oils, at a much higher concentration. The reworked oil content in the EE formulation can be increased drastically without compromising other emulsion properties. Figure 4 represents the stability of EE at higher reworked oil content whereas Figure 5 shows the improved sleep time stability. It is worth mentioning that besides the fact that EE (with radical increase of reworked oil in the fuel phase formulation) showed acceptable stability on shelf, the optimised surfactant system improves the sensitised and doped emulsion explosives' sleep

EE stabilised with optimised surfactant system and radical increase of used oil in the fuel phase

EE stabilised with conventional surfactant system and standard content of used oil in the fuel phase

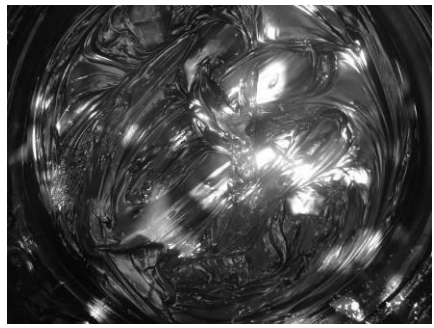

Figure 4. EE stability at increased reworked oil content (radical increase of used oil in the fuel phase) after 30 days of storage.

time stability with lower degree of EE performance drop over 6 week sleep time period (Table 3). It can clearly be seen from Table 3 that the emulsion, stabilised by the optimised surfactant system, showed higher velocity of detonation (VoD), which was also more consistent when compared to the conventional surfactant system. The higher VoD phenomenon can be explained by the better sensitisation quality which is reflected by the size of the gas bubbles that are created during the chemical reaction of sensitisation. The difference in the gas bubble size for different emulsion formulation stabilised by different optimised co-surfactant system is represented in Figure 6.

Furthermore, the recent tendency of converting to the usage of diesel with a lower sulphur number caused some instability to EE. This instability was caused due to the presence of diluents and chemicals used to reduce the sulphur content in 50 ppm diesel grade when compared to 500 ppm diesel grade. The instabilities are mainly associated with emulsion explosives droplets coalescence that can be determined microscopically (presence of big droplets) and visually (drop of base EE viscosity). The optimisation of surfactants system allows extending the limits of the tolerance to the solvents present in the 50 ppm diesel grade. Figure 7 shows the coalescence of EE when emulsion was stabilised with conventional surfactant system and a more stable system with no signs of the coalescence for EE stabilised with optimised surfactant system.

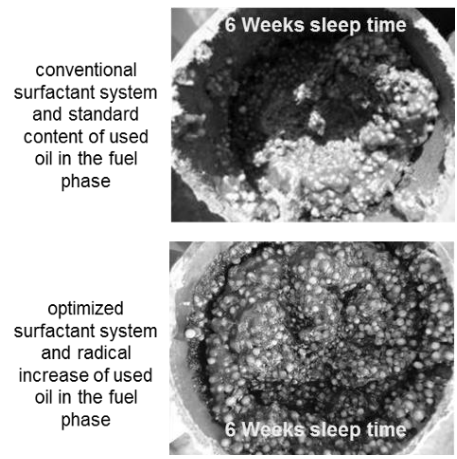

Figure 5. Improved sleep time stability of sensitised and doped EE.

The over gassing resistance of doped sensitised emulsion explosives was tested for the EE stabilised with conventional and optimised co-surfactant system. It was found that EE stabilised with optimised co-surfactant system showed no sign of collapse or breakdown with ANPP being intact in harsh over-gassing test conditions (Figure 8).

4 SUMMARY AND CONCLUSIONS

Within the frame of our experimental work, it was

Table 3. EE performance after 6 weeks of sleep time in cardboard pipes.

Emulsion explosives	Velocity of detonation, m/s	
	Initial	After 6 weeks of sleep time
stabilised with conventional surfactant system and standard content of used oil in the fuel phase	4050 - 3850	3450 - 3050
stabilised with optimised surfactant system and radical increase of used oil in the fuel phase	4390 - 4340	3832 - 3852

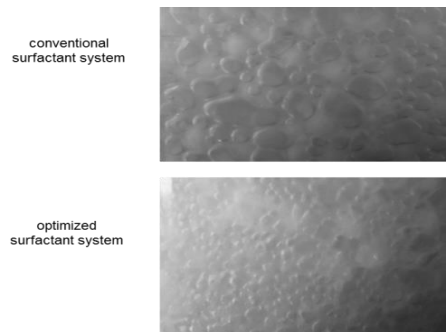

Figure 6. Comparison of sensitised emulsion gas bubble size.

shown that the conventional surfactant system has limitations. The limits can however be extended by optimising the surfactant system and adjusting the EE parameters based on the customer's request. The implementation of the optimised system of co-surfactants allowed: (i) the optimisation of the level of actives in the fuel phase of the emulsion formulation; (ii) the use of lower grade fuels (including different grades of diesel); (iii) the improvement of the carbon footprint; (vi) the improvement of the emulsion explosives' stability on shelf and in pumping; (v) the improvement of the emulsion explosives' sleep time in the blast-hole; (vi) the

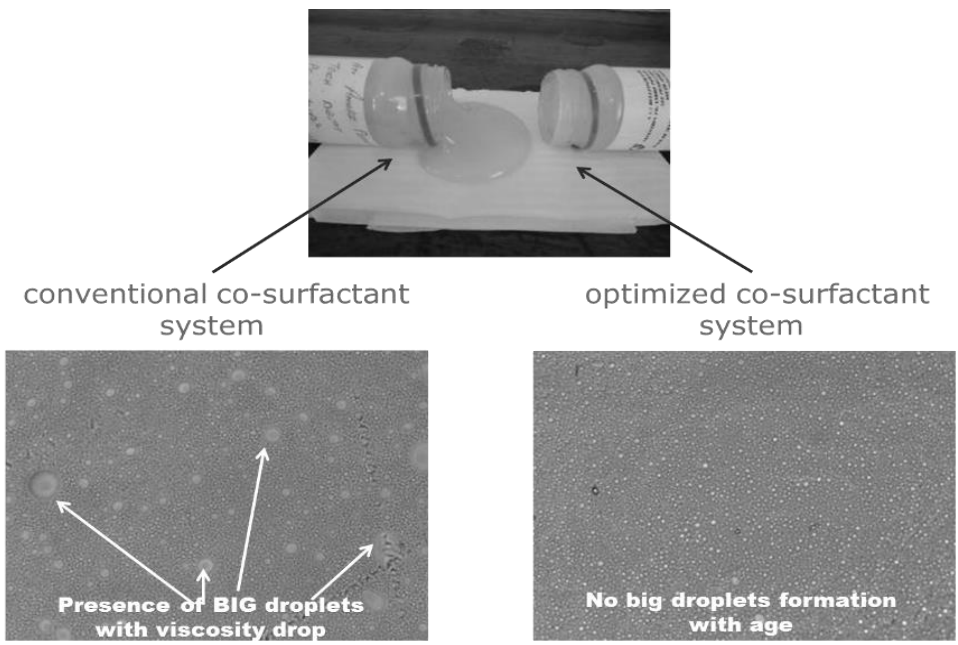

Figure 7. Stability of emulsion to coalescence with low sulphur content diesel in the emulsion formulation.

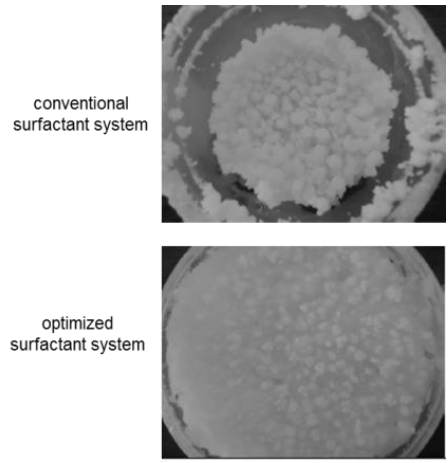

Figure 8. EE over-gassing test results (after 24 hours of testing).

improvement of emulsion explosives' blast performance.

REFERENCES

Becher, P. 1985. *Encyclopedia of emulsion technology*, Vol. 2, Applications, Derek, New York, 1985.

Drelich, A., Gomez, F., Clausse, D. & Pezron, I. 2010. *Colloids and Surfaces*, vol. 365, p. 171.

Hunter, R.J. 1986. *Fundamentals of Colloid Science*: Vol. 1, Oxford Science, 1986.

Hunter, R.J. 1993. *Introduction to Modern Colloid Science*, Oxford Univ. Press, 1993.

Kim, J., Lee, D., Shum, H.C. & Weitz, D.A. 2008 *Advanced Materials*, 2008, vol. 20, p. 3239.

Masalova, I., Malkin, A.Ya., Ferg, E., Kharatiyan, E., Taylor, M., Haldenwang ,R. & J. Rheol. 2006. Vol. 50 (4), p. 435.

Masalova, I. & Malkin, A.Ya. 2007. *Colloid Journal*, 2007, vol. 69, no. 2, p. 220.

McClements, D.J. 1995. Food emulsions: principles, practice and technologies, CRC Press, 1999.

Schramm, L.L. 1992. *Emulsions: Fundamentals and Application*, Am. Chem. Soc., 1992.

Tshilumbu, N.N., Ferg, E.E. & Masalova I. 2010. *Colloid Journal*, 2010, vol. 72, no. 4, p. 569.

Stockholm Conference Proceedings 2017, R. Holmberg et al

Explosive cutting of pipelines for the determination of materials properties

K. Holtappels & B. Theil
Bundesanstalt für Materialforschung und –prüfung (BAM), Berlin, Germany

M. Erdelen-Peppler & K.C. Meiwes
Salzgitter Mannesmann Forschung GmbH, Duisburg, Germany

ABSTRACT: Incidents in the past already showed that pipelines transporting compressible fluids are at risk of suffering propagating ductile fractures in case of damages to the pipes. Therefore, the knowledge of the fracture properties of pipeline steels is of high importance. Commonly the properties are determined in laboratory scale, but these do not fully correspond with full-scale fracture behaviour especially at dynamic conditions when highly pressurised gases are released during the crack propagation. This paper describes so-called West Jefferson Tests and Midscale Tests in which pipelines under pressure were cut with an explosive charge to initiate the crack propagation.

1 SAFETY OF PIPELINES

Oil and gas provide 60% of the world's primary fuel and a large proportion is transported in pipelines. The pipelines are designed, built and operated to well established standards and rules, because the products they carry can pose a significant hazard to the surrounding population and environment. A combination of good design, adequate material properties and sound operating practices are therefore necessary, to ensure that transmission pipelines operate safely and efficiently.

Incidents in the past showed that pipelines transporting compressible fluids are at risk of suffering propagating ductile fractures in the case of damages to the pipes. Foremost, it is important to guarantee for ductile fracture propagation whilst excluding brittle propagating fractures. Although the Drop Weight Tear tests (DWTT) have emerged as the most suitable laboratory test to substitute for full scale tests on pipes to assess the fracture surface of fractured pipes, a lot of data exist for another laboratory scale tests called Charpy V tests. Unfortunately, the results of both tests often show deviations with respect to the resulting transition temperatures. A validation is finally required based on large scale tests, in which pipelines are set under pressure and cut by an explosive charge in order to initiate a

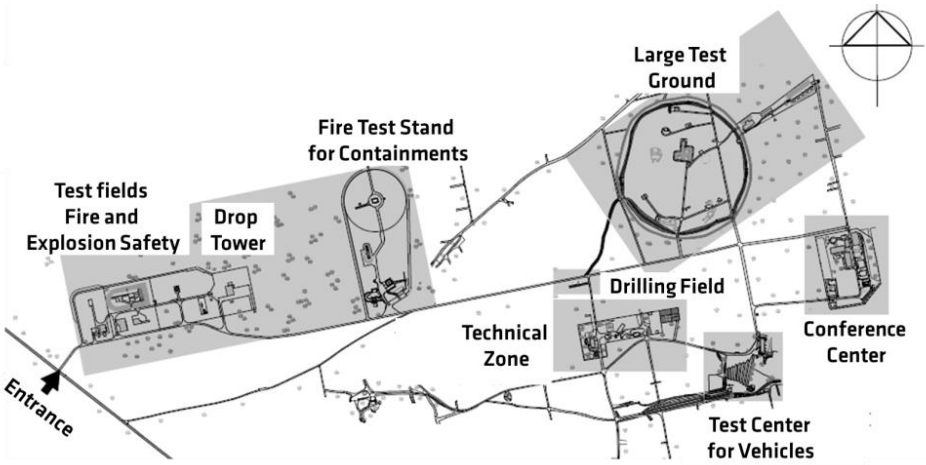

Figure 1. Schematic view of BAM test site technical safety (TTS).

crack propagation.

This paper describes the procedure and results of pressure vessel fracture tests called West Jefferson and/or Midscale Test. The main difference between both tests is the temperature at which the pipeline is cut. West Jefferson Tests are carried out at low temperatures, for which the pipelines have to be cooled down. Midscale Tests are carried out at ambient temperatures.

2 EXPERIMENTAL

2.1 Location of explosion tests

All tests were carried out at the BAM Test Site Technical Safety (TTS, Figure 1), located in Baruth/Mark, 60 km south of Berlin. The test site is 12 km² and consists of various main facilities to carry out large scale tests.

Figure 2. Aerial view of the large test ground with a diameter of 400 m.

At the centre of the site is an explosion test ground with a diameter of 400 m. A protection wall surrounds the test ground. Officially, BAM is allowed to ignite max. 150 kg TNT. Therefore, the test ground is the largest non-military test site for such tests in Europe. Figure 2 presents a picture of the test ground taken by an unmanned air vehicle (UAV). The explosion test ground includes fixed installations to carry out not only tests with explosives, but also to carry out large scale fire tests with substances, containments, devices and/or plant components.

2.2 Tested pipelines

The pipelines, provided by Salzgitter Mannesmann Forschung GmbH and delivered to the test site, were prepared for the West Jefferson Tests. Metal boxes were welded on top of the pipelines to keep the cooling liquid ethanol (Figure 3a). Further installations in the box realized the introduction of liquid nitrogen to cool down the required area of the pipeline to the requested temperature at which the initial crack and its propagation should be initiated. The ethanol guarantees a uniform and softer cooling of the pipeline than putting liquid nitrogen directly to the top part of the pipeline.

The Midscale Tests were carried out at ambient temperatures, but with 36 m long pipes. Nevertheless, the most important pipe part was the centre part. The additional 12 m pipes at each side are required to have a large reservoir of pressurized air which forces the crack propagation after cutting. These pipes, finally welded at the test

ground, were placed in a dig in order to limit the movement of pipe parts during the test. Furthermore, additional weight was placed at the end of the pipe for the same reason (Figure 3b).

Figure 3a. Pipeline for West Jefferson Test.

Figure 3b. Pipeline for Midscale test (placed in a dig).

Figure 4. Preliminary tests with various cutting charges to guarantee a safe crack initiation (top pictures: cutting of 25 mm thick walls; bottom pictures: cutting of 38 mm thick walls).

2.3 Cutting charges

Dependent on the wall thickness of the pipes (25 mm respectively 38 mm) cutting charges were chosen to initiate a first cut of the pipelines safely. In preliminary tests the efficiency of the various charges was tested ahead (Figure 4). Table 1 presents the cutting charges finally used for the tests.

Table 1. Properties of used extended, flexible cutting charges on basis of PETN (nitropenta)/RDX (hexogen) used to initiate crack propagation in pipes with different wall thickness.

	Semtex RAZOR 25	Semtex RAZOR 40
Cutting capacity, referred to steel St 37 (mm)	25	40
Mass of explosive (g/m)	860	2200
Total mass (g/m)	2400	6000
Density of explosive (g/cm³)	1.56	1.56
Detonation speed (m/s)	7500	7500

Figure 5. Placement of the cutting charge for the West Jefferson Test in a protected area (no contact to the cooling liquid).

For the West Jefferson test and the Midscale tests cutting charges with a length of 500 mm were

Figure 6. Picture sequence of a West Jefferson Test (pipe length of 8 m, wall thickness of 38 mm, initial pressure of 300 bar, initial temperature of -20°C).

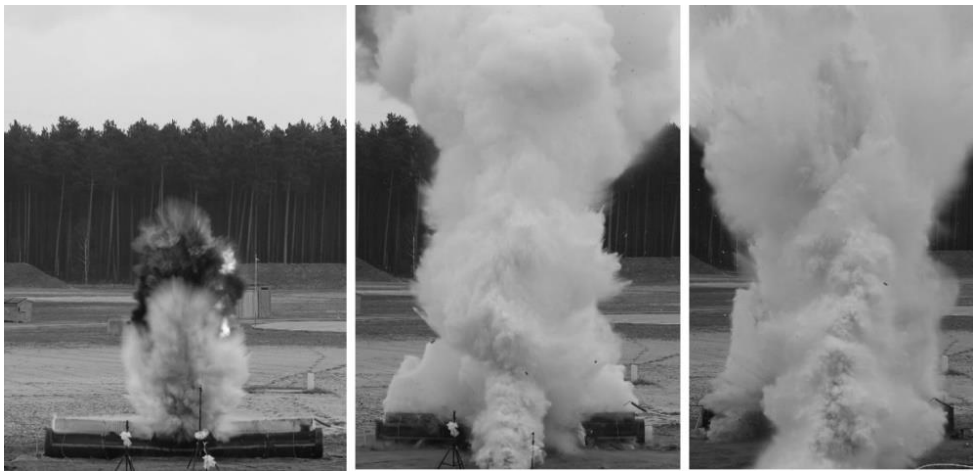

Figure 7. Picture sequence of the second West Jefferson Test (pipe length of 8 m, wall thickness of 25 mm, initial pressure of 180 bar, initial temperature of -30°C).

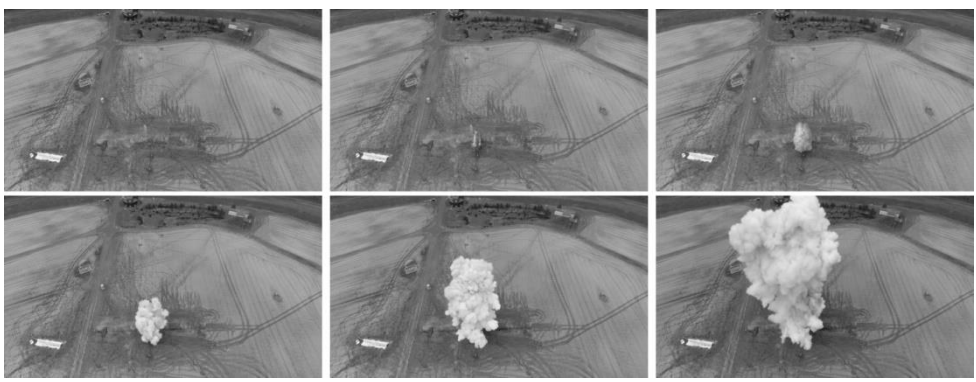

Figure 8. Picture sequence of the Midscale Test, taken with a UAV (pipe length of 36 m, wall thickness of 21 mm, initial pressure of 300 bar, ambient temperature).

Figure 9. Picture of the pipeline after the first West Jefferson Test (pipe length of 8 m, wall thickness of 38 mm, initial pressure of 300 bar, initial temperature of -20°C).

applied to a centre part of the pipeline. In case of West Jefferson Tests the centre part had to be protected so that the ethanol used to cool down the pipeline partly did not get in direct contact with the cutting charge. Figure 5 demonstrates the final application of the charge to the pipeline.

3 TEST RESULTS

Two West Jefferson Tests and one Midscale Test were carried out at the test ground. At first, pressurised air was introduced to the pipelines. This took up to 22 hours in case of the Midscale test although the compressor used was able to compress 630 l/min. Once the initial pressure was reached, the cutting charge was placed to the pipeline and ignited.

Picture sequences and the cut pipelines respectively the final cracks are shown in Figures 6 to 8. Due to the enormous pressures inside the release is accompanied by large white clouds formed by condensing air humidity.

After each test pictures were taken of the ruptured pipelines. Special care was taken for the cut parts. Figures 9 to 11 show the pipelines after the tests. The initial cracks initiated by the cutting charges can be seen and are clear to differentiate from the cracks propagated from the edges of the cutting charges. The crack propagation length was dependent on the pipeline material, its wall thickness, the material temperature and the inside pressure, of course. A detailed analysis of the cut pipeline parts was done by Salzgitter Mannesmann GmbH and is not part of this paper.

Figure 10. Picture of the pipeline after the second West Jefferson Test (pipe length of 8 m, wall thickness of 25 mm, initial pressure of 180 bar, initial temperature of -30°C).

4 SUMMARY

Although well-defined, laboratory scale tests exist in order to determine important material properties of pipeline materials large scale pressure vessel fracture tests called West Jefferson and/or Midscale Test are useful to validate the properties. Such validations are required to ensure that transmission pipelines operate safely and efficiently for long times and at their ambient conditions.

Figure 11. Picture of the pipeline after the Midscale Test (pipe length of 36 m, wall thickness of 21 mm, initial pressure of 300 bar, ambient temperature).

In order to carry out reliable large scale pressure vessel fracture tests explosives are required to initiate the initial crack safely. Furthermore, the crack, induced by the cutting charges, must be clearly distinguishable from the crack which develops in the further course, which spreads through the internal pressure. Otherwise the determination of the intended material properties would not be possible.

REFERENCES

Hillenbrand, H.G., Liessem, A., Kalwa, C., Erdelen-Peppler, M. & Stallybrass, C. 2008. Technological solutions for high strength gas pipelines. *Proceedings of International Pipeline Steel Forum.* Peking.

Pistone, V., Demofonti, G., Junker, G. 2000. Transition temperature determination of thick wall line pipes. *3R International: 199-204.*

Holtappels, K. 2016. Materialuntersuchung an pipelinerohren unter einsatz von schneidladungen. *Seminar on Explosives and Pyrotechnics*. Berlin.

Stockholm Conference Proceedings 2017, R. Holmberg et al

A new approach to blasting services contracts

R. Tamir
Lead consultant, Seekers Strategic Solutions

ABSTRACT: Muck-pile density, profile and fragmentation have a far-reaching downstream impact. Measuring and understanding the cause and effect of the blasting is a key to pushing the performance envelope and value creation. Technologies such as *fragmentation photo analyses* of the muck-pile, HME and process performance are already in place. We can accurately quantify and correlate blasting parameters and re-structure the blasting contracts to create downstream value – *Get a bigger bang for the buck*. This paper will describe the method, tools and the added value of this approach. As our ability to monitor and control the blasting loading, hauling and processing of ore we can utilise these capacities to make a major downstream contribution and an economical impact by defining the blasting services contract better and allocation accountability and cause & effects to the rightful owner and jump starting a Continuous Improvement process.

1 METHOD DESCRIPTION

Our ability to accurately quantify and evaluate the blasting and its outcome allows the setting of clear blasting goals that support the operation in a number of ways.

1.1 Providing data relevant to the outcome

Providing the blasting crew accurate data relevant to the required outcome would include:

- rock properties based on technology drills poses (ether inherently or attached) creating the capacity to report hole data - top and bottom colour locations, drill penetration rate (that indicates rock property changes and deviations) by measuring penetration rates amongst other items
- determination of geological structure, contacts, bedding planes and caustic activity, based on drill penetration rate data to support the blast planning. The drill manufactures and providers of data performance made an honest and successful effort to provide drilling performance data in real-time

1.2 Providing fragmentation and muck-pile targets

Providing the blasting crew with clear fragmentation and muck-pile targets based on mining and processing equipment parameters by providing the following:

- fragmentation in the mock-pile by location
- pile density and dig-ability, this data is used to indicate the effort and the efficiency of the

mining equipment and the compatibility of the pile to the mining equipment

- completability (*sic*) to process stations
  - entry point – large size limit, size distribution (for maximizing the process efficiency)
  - downstream process – for maximizing process effectiveness
  - final product – for reducing cost and the ability to bypass some of the process components

1.3 Muck pile monitoring

Monitor the muck-pile spread, density, height and fragmentation by location in the pile by providing drone generated data indicating the effectiveness of the blasting according to the set targets and benchmarks. This data coupled with the blast planning tools allows operators to take the necessary steps as a part of a continuous improvement process aimed at pushing the blast performance (blasting cost effective solutions) envelope.

1.4 Simulation

Simulation of process performance, including load and haul, correlated to the blasting results.

1.5 Compatibility

Continuously evaluate the compatibility to process and impact on final product thru KPI (including KPI validation process) and floating targets based on scenarios.

1.6 Tools for continuous improvement

The tools are divided into two groups. Firstly 'data', which includes collection, analysis and the Continuous Improvement process. Secondly, contractual tools.

1.6.1 Data collection tools

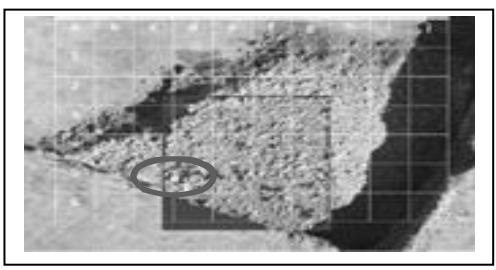

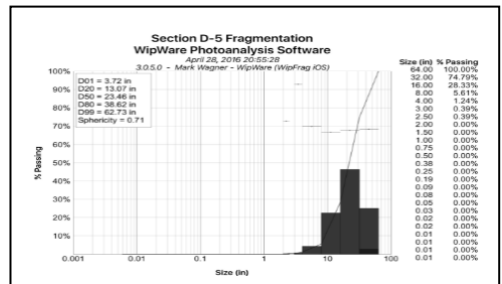

Figure 1. Analysed drone generated imagery.

Process monitoring tools – bet scales, fragmentation photo analysis devices, mobile equipment performance monitoring (loading, hauling, drilling equipment, data collection).

1.6.2 Data analysis tools

Tracking, trending and correlating cause and effect. Those tools are used by all involved and assist in creating a true fair bench-line. As the data is accurate and detailed it is clear that the bench-line is a floating one as the geology and ore parameters change.

1.6.3 Continuous improvement process

An additional tool is the Continuous Improvement process. The abundance of data allows the mine to continuously push the performance by pushing the blasting impact downstream. This concept doesn't necessarily imply cost saving in drill / blast operations. In many instances the opposite is true.

1.6.4 Contractual tools

The contractual tools are a set of formulas set by guidelines based on the data and both the mine and the service provider are committed to using and abiding by them for example:

- for each variance in in-situ ore properties a sliding target is in effect – since we strive to maximise the fragmentation downstream effect in some location the blasting parameters such as pattern, hole diameter, use of accessories and type of explosive will differ. The blasting service provider is held accountable to achieve a cost-effective solution within x time and as long as conditions stay the same;
  - the price stays the same

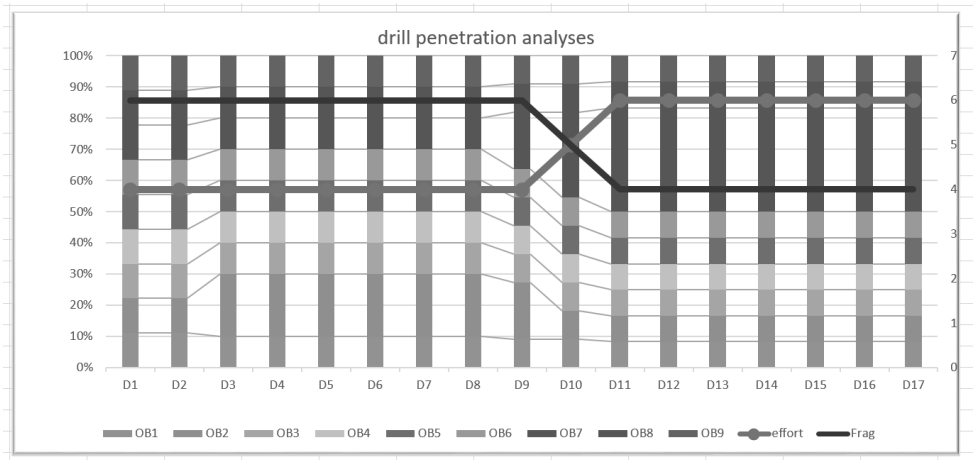

Figure 2. Drill penetration data providing rock strength property change.

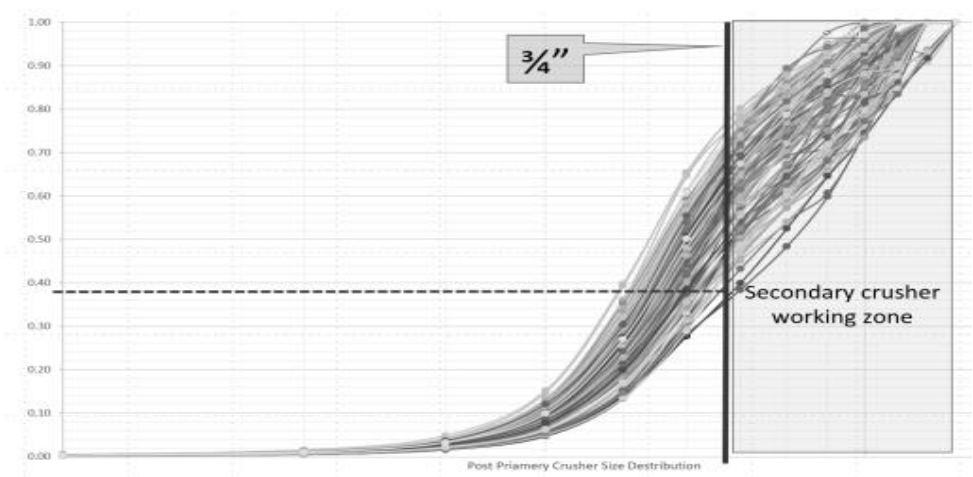

Figure 3. Tracking particle sizes as they pertain to the secondary crusher specifications.

- the performance stays as good, any variation from the performance level due to the service provider's actions results in a penalty
- the mine, must share all data with the service provider in order to allow him to perform as best as possible

As we can create a ***situational awareness*** (a highly reliable, well-balanced knowledge level picture) by integrating and correlating the data from pit to mine a blasting contract that reflects the value can now be tailored to a much-detailed list of parameters such as fragmentation targets, pile density and fines generation.

This contract will include a higher level of input to assist the drill and blast crew to allow them to meet their targets and create higher value for the mine.

This approach allows the attribution of accountability for performance, good or bad, at the feet of the rightful owner with the intent to learn and push the performance envelope.

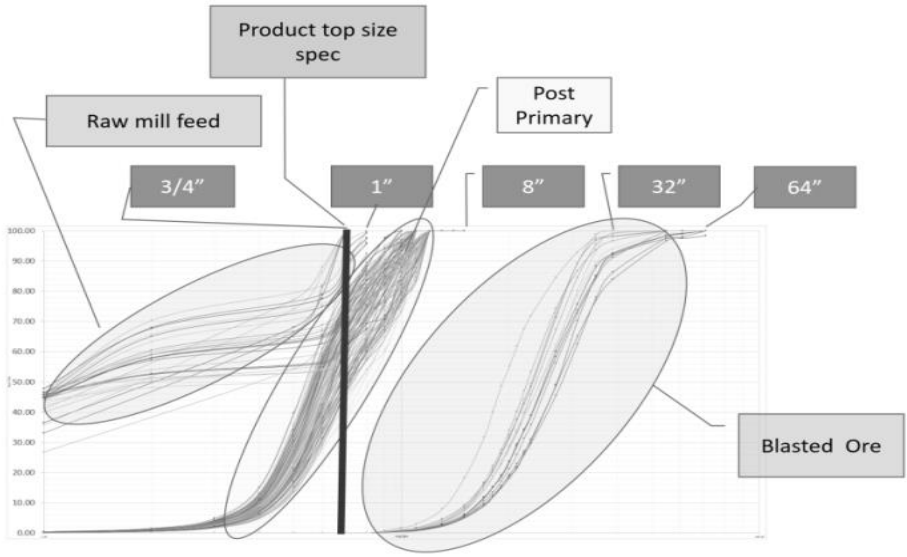

Figure 4. By comparing the fragmentation data from the blasting and crushing zones tracked, we can begin to identify the contribution that each phase makes.

Table 1. Bench marking of dig-ability and process indicators.

Source	material	type	T/BCY	digability factor		fragmentation benchmark (in inches) %passing			
				fuel usage gl /cycle	bucket fill	32	16	12	1/8"
		Ore/IPW	2.23	-0.25	110%	100.00%	90.00%	80.00%	5.72%
		waste	1.49	-0.25	100%	100.00%			
		Ore	2.29	-0.25	110%	100.00%	90.00%	80.00%	5.72%
		waste	2.29	-0.25	100%	100.00%			
		Ore/IPW	2.23	-0.25	110%	100.00%	90.00%	80.00%	5.72%
		waste	2.23	-0.25	100%	100.00%	90.00%	80.00%	5.72%
		Ore/IPW	2.23	-0.25	110%	100.00%	90.00%	80.00%	5.72%
		Ore/IPW	2.23	-0.25	110%	100.00%	90.00%	80.00%	5.72%
		Ore/IPW	2.23	-0.25	110%	100.00%	90.00%	80.00%	5.72%
		Ore/IPW	1.49	-0.25	110%	100.00%			

Note to table: All handling of all material +32 in. in a timely manner in coordination with Quarry management at vendor’s expense. Bucket fill calculation based on registered bucket load and agreed upon loose density of material for every additional 3% increase in fines (per the entire shot) the vendor will grant a 5% discount from the total shot cost, up to a maximum of 20%. Two shots of over 20% fines will be considered a breach of contract.

2 CONCLUSIONS

Measurement, simulation, analytical tools together with enhanced blasting abilities – electronic initiation, variable density emulations allows improved blasting performance. Most current blasting contracts do not create additional measurable value for the clients. Our approach proposes tools and methods to achieve higher value.

Utilising this approach it is possible for both the mine and the blasting services provider to profit, the first by reducing overall cost and the second by enhancing (changing) its revenue through providing added value.

This approach allows tighter control over the blasting performance and through sharing data it is possible to 'hold the service provider's hand to the fire' to be accountable for value and not just for the blast.

This approach is gaining traction with mining companies and the structure of the blasting services bids are changing.

It is wise, on the service providers part, to take the initiative as then they lead the process and can gain advantage by utilising technology verses pounds as technology is cheaper.

3 RECOMMENDATIONS

- build the contracts based on value not on pounds. The expression of value is expressed in the table.

Table 1 is an extract from the contract, bench-marks performance indicators such as loading equipment fuel usage indicating dig-ability of the muck-pile and fragmentation indicating dig-ability and process efficiency.

- change the relations between the planner, drill, blast, QC, production and process phases from siloes to an integrated target oriented relationship
- installing a rigid process of continuous improvement and learning
- use the tools & methods to tailor a site specific solution capable of measuring progress and success
- establish site specific downstream KPI and process
- be willing to pay higher D&B cost for a higher downstream contribution on one hand and not compromise on poor measurable blasting results

Stockholm Conference Proceedings 2017, R. Holmberg et al

Innovation in up-hole deviation measurements in sublevel stoping mines

J. Orive, R. Laredo, J.F. Domingo & J. Sadek
Maxam Europe S.A., Minas de Aguas Teñidas, S.A.U., Huelva, Spain

ABSTRACT: Technological mining advances in the twenty-first century have enabled the viability of some projects worldwide which a few decades ago were considered uneconomical. Deviation of holes related to their projected design, results in great costs and safety problems. Drilling accuracy may impact the efficiency of the project (*i.e.* mineral recovery in the stopes, dilution control and blast damage stability), explosive consumption and fragmentation size. Drilling deviations from the designed drill pattern are responsible for deficiencies in blast results. This can generate overbreak (dilution), underbreak (losses) and blast damage which have a negative impact on the economic results and generate instability, operational and safety problems. In the 'Faja Pirítica' (the Pyrite Belt in the South of Spain), the charging of blast holes in 360˚ rings is being developed in several underground mines. For the execution of these works, carriers equipped with automated pumping units are used to ensure effective filling of the holes. A new measuring system has been incorporated into explosive charging units to monitor the accuracy of drilling. The innovation of the project is the implementation of a sensor coupled to the hoist so measurements are taken automatically while placing the booster into the hole. To date, the system has been used to monitor 30 holes in which the measured deviations at the end of the hole were found to be 15±5 % of the blasthole length (mean and standard deviation). This tool is the starting point for the establishment of a QA / QC system to achieve operational excellence and take front-line decisions to reduce drill holes deviation, modify designs or explosive types. Further testing is planned in other mines to validate the system.

1 INTRODUCTION

Technological advances in blast design software and the greater accuracy in topographic measurements in underground mines have enabled, over recent decades, substantial improvements in the spacial location of blast holes. Also, positioning systems of drilling equipment reduces collar location error, as well as other errors like direction and hole length.

Common errors in drilling operations include collar location and direction setting. However, unknowns persist over the path and end point of the actual drill hole. In many instances, post-analysis results of blasting performance, ore recovery and geometry of the stope can only be explained by the effect of hole deviation with respect to the design (Figure 1).

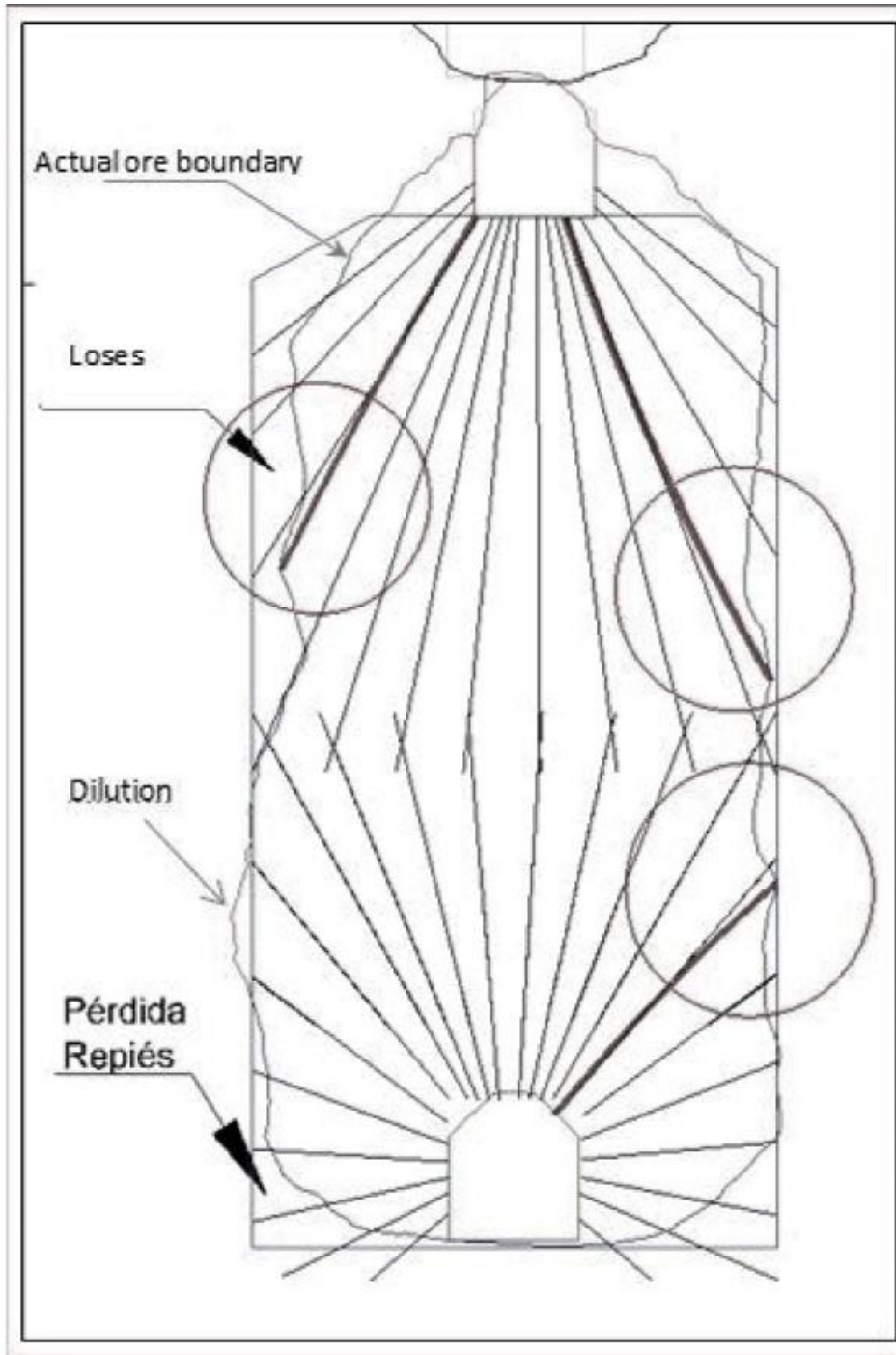

Figure 1. Blast hole path deviation from design.

It is known that the deviation is caused by numerous factors such as: drill rod diameter, drill penetration rate, rock geology and drilling experience (Orpen 2005).

Although the economic value of the losses produced by this effect may be very high, it is difficult to find investigative probes that are adapted to the needs of the mining industry, particularly those which evaluate upward blast holes of stopes.

Figure 2. Riosensor deviation measurement system.

In many cases, this is due to the technology used (gyroscopic or magnetometric systems) and the high cost involved in measuring the deviation (both in mechanical and human terms).

Maxam has developed a system of surveying drill hole deviation (Figure 2), which incorporates the sensor in the up-hole charging unit with the objective of measuring the deviation automatically.

2 MAXAM SERVICES AT AGUAS TEÑIDAS MINE

Maxam provides PUMP AND GO services at MATSA's mines for blast holes drilled in 360º rings (Figure 3).

In addition, a drill checking service is provided, which consists of a detailed report of the condition of the drill holes prior to loading, indicating the presence of blockages, total lengths and deviations of the trajectory.

The UG bulk units have incorporated a probe coupled to the hose that is inserted in the blast hole. A pusher element guides the probe on its way to the end of the blast hole, measuring points with an encoder device every 2 metres.

The lifting arm of the crane raises the measuring equipment in order to align it with the blast hole, then the automatic hose pusher is engaged, inserting the instrument to the end of the blast hole while surveying (Figure 4).

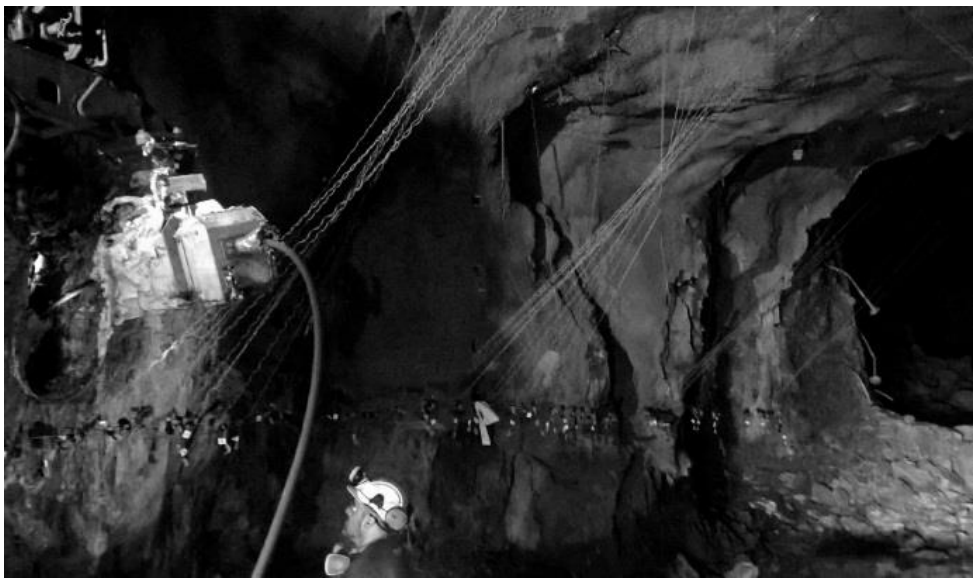

Figure 3. Charging of blast up-holes.

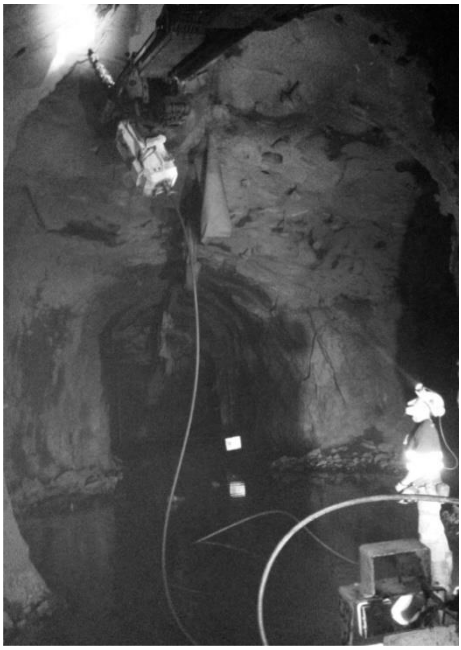

Figure 4. Blast hole surveying.

The probe collects readings of azimuth, inclination, temperature of the sensors and components of the gravitational and magnetic fields.

Communication software enables processing of the information collected by the probe and it is validated by the operator in real time (Figure 5).

According to the fundamentals of probe operation, when the inertial sensors are affected by accelerations due to the movement of the equipment, or local magnetic interactions interfere with magnetometers, the inclination or azimuth values are rejected.

The results of the measurements in each hole are shown in Table 1.

- length error: measured length - design length
- tilt error: inclination measured at 3m - actual inclination
- azimuth error: azimuth measured at 3m - actual azimuth
- deviation error in x, y, z: end point of the actual blast hole - end point of the designed hole

Figure 5. Survey validating process.

Each blast hole shown in Table 1 is graphically represented according to sections S-N and W-E (Figures. 6a and 6b).

However, other kinds of representations can be made according to the axis of the gallery in which the holes are drilled in a radial pattern around the drive. This facilitates the visualisation of the losses or increases of actual burden and spacing in relation to that of the design.

Table 1. Measurement results in Stope AL 900-850.

Date: 8/3 2017		Depth (m)			Inclination (º)			Azimuth (º)			Blast hole end offset (m)		
stope	BLAST HOLE	measure	design	error	measure	design	error	measure	design	error	delta x	delta y	delta z
AL 900-850	b0106	18.2	17.0	1.2	151.7	152.6	0.9	174.8	171.0	3.8	0.0	-2.0	0.3
	b0107	19.1	19.2	-0.1	144.7	148.8	4.1	175.8	171.0	4.8	0.2	-1.8	-1.4
	b0108	21.7	20.3	1.5	140.5	144.3	3.8	172.5	171.0	1.5	0.4	-2.9	-0.6
	b0110	22.3	22.9	-0.6	132.5	135.9	3.4	174.6	171.0	3.6	-0.8	-1.8	-2.8
	b0112	22.3	23.4	-1.1	124.8	128.2	3.4	177.0	171.0	6.0	-1.8	-1.0	-3.0
	b0113	20.1	22.5	-2.4	123.2	121.0	2.2	175.2	171.0	4.2	-1.1	-1.9	1.7

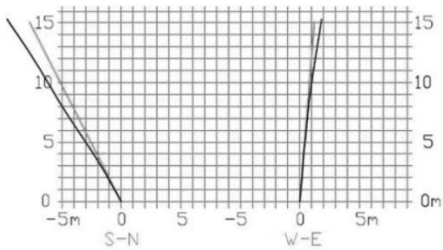

Figure 6a. Graphic representation according to S-N and W-E sections.

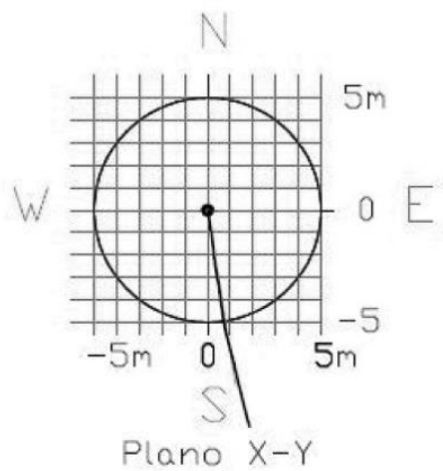

Figure 6b. Graphic representation according to N-S and W-E sections.

Three-dimensional representation of the planned and measured holes highlights the deviation encountered (Figures 7a and 7b).

3 ACCURACY AND MODEL CONFIDENCE

One of the main limitations of drill measurement probes is to demonstrate the accuracy and precision of the results compared to design parameters.

Values returned by the probe without taking into account errors produce an accumulative effect on subsequent measurements. The pathway of the hole is determined by adding vectors between measurement points; the start point of a new vector is the end point of the previous. Non-validated data could lead to inaccurate results.

In order to compensate for out-of-range readings and improve accuracy, measurements are taken along the blast hole from collar to end, and then are also taken as the hose is withdrawn from hole end to collar.

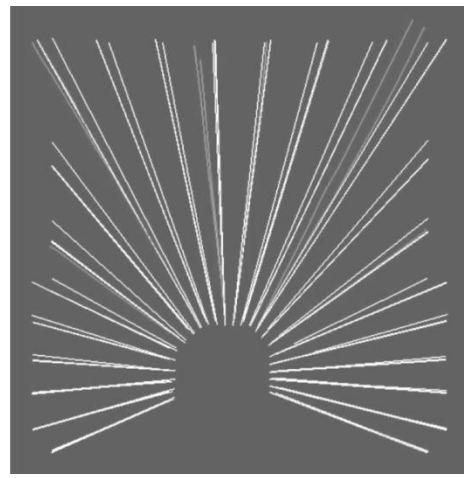

Figure 7a. Graphic representation in 3D views.

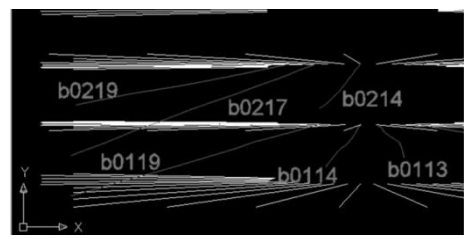

Figure 7b. Graphic representation in 3D views.

Some of the random and systematic errors that the system faces are:

- error of alignment with the axis of the borehole by the presence of detachments or voids in it, tangential forces due to the thrust of the hose or deformation of the probe centre. To avoid this, as a general rule, measurements are made on drill holes which have been previously checked. In addition, the join between the hose and the probe has a cardan coupling that prevents lateral distortion and the centring devices are replaced regularly.

Table 2. Rejection of non-valid readings.

VALUE	Time Stamp (sec)	Inclination (º)	Azimuth (º)	Dip Angle	Accel Temp (ºC)	Mag Temp (ºC)	GTOT (m/s)	HTOT (gauss)
REJECT	0.5	151.684	175.01	40.427	27	26.5	1.001	0.4
REJECT	1	150.176	174.724	55.273	27	26.5	0.998	0.461
OK	1.5	149.119	180.265	54.607	27.2	26.5	0.994	0.493
OK	2	148.059	172.93	53.151	27	26.5	0.994	0.486
OK	2.5	148.005	181.374	51.156	27.2	26.5	1.008	0.482
OK	3	146.377	180.933	51.034	27	26.5	1.011	0.479

- depth position error: failures in the pusher device and the meter, by sliding the hose without turning the encoder. This is reduced with regular maintenance and calibration
- device error: the inherent accuracy of the device according to the manufacturer's specifications. This error is minor compared to the rest of magnitudes.
- error from local magnetism: the presence of ferromagnetic elements produces a proximal disturbance in the terrestrial magnetic field that distorts the readings. As a general criterion, adopted by the Geology Department at Matsa, a default value of the magnetic decline is set at -3º as a flag. To discriminate readings affected by local magnetic field alterations, the probe measures a control variable at each station, which is the angle between the geomagnetic field vector and the gravity vector. In absence of local anomalies, this angle depends on the geographic latitude. If the reported angle in this mining area is significantly different to the expected figure, 52º+/- 5%, it is then likely that a magnetic interference exists, or a linear acceleration occurred during the measurement, or that the device is not operating correctly.

As an additional consideration, statistical monitoring of the records is performed, analysing their variability and checking independently if the values of G and H keep between a range of +/- 5% of their reference values in the area that are 9.8 m/s and 0.48 Gauss. This leads to automatic rejection of those outliers, as shown in Table 2.

Periodically a calibration of deviation measurement is performed, consisting of sampling 'draft' drill holes. That is, the topographical measurement of those blast holes which break through to an accessible mine area above or below the collar location. Measurements taken by both topographic and probe methods are compared in Table 3.

Table 3. Control measure accuracy.

		Blast hole end offset (m)		% error
Length (m)	delta x (m)	delta y (m)	delta tot (m)	
17.0	-0.21	-0.28	0.35	2.05%
18.5	-0.10	-0.45	0.46	2.49%

All of the above mentioned issues lead to the conclusion that the method can be calibrated to confidently reflect actual drill hole performance.

4 ECONOMIC IMPACT IN A MINING PROJECT

Through the collection of data in various mining projects, Maxam has created a statistical model applicable to any mining project, with the objective of quantifying the economic impact of borehole deviation.

This model is based on analysing the deviation values of a set of surveyed blast holes and comparing them against design.

In this case, statistical evaluation of the data set collected demonstrates (in Table 4):

Table 4. Deviation actual vs design blast holes.

BLAST HOLE	Depth (m)			Inclination (º)			Azimuth (º)			End offset (m)			Error
	Mea-sure	Design	Error	Survey	Design	Error	Survey	Design	Error	Δ X	Δ Y	Δ Z	Total (m)
B0106	18.2	17	1.2	151.7	152.6	0.9	174.8	171	3.8	0	-2	0.3	2.02
B0107	19.1	19.2	-0.1	144.7	148.8	4.1	175.8	171	4.8	0.2	-1.8	-1.4	2.29
B0108	21.7	20.3	1.5	140.5	144.3	3.8	172.5	171	1.5	0.4	-2.9	-0.6	2.99
B0110	22.3	22.9	-0.6	132.5	135.9	3.4	174.6	171	3.6	-0.8	-1.8	-2.8	3.42
B0112	22.3	23.4	-1.1	124.8	128.2	3.4	177	171	6	-1.8	-1	-3	3.64
B0113	20.1	22.5	-2.4	123.2	121	2.2	175.2	171	4.2	-1.1	-1.9	1.7	2.78
A5B12	12.5	12.4	0.1	144.7	144.8	0.1	79.8	80	0.2	-0.6	0.8	0.3	1.04
A5B13	8.7	8.9	-0.2	131.6	132.3	0.7	84.3	83.6	0.7	-0.3	-0.1	0.1	0.33
A5B15	7	7.3	-0.3	98.1	98.2	0.1	89.2	89	0.3	-0.3	0.1	-0.3	0.44
A6B3	21.2	20.4	0.8	167.1	164.1	3	301.4	299.5	1.9	1.3	0.4	1	1.69
A6B6	20	20	0	167.8	167.2	0.6	48.1	51.6	3.6	-1.4	1.2	-0.1	1.85
A6B7	21.3	20.7	0.6	160.1	160.4	0.3	66.2	66.8	0.6	-1.4	2.3	0.4	2.72
A6B8	22	22.1	-0.1	156.8	153.1	3.7	73.8	73.9	0.1	-2.6	2.1	0.4	3.37
A7B2	17.1	19.9	-2.8	161.6	165.2	3.6	305.5	307	1.4	1.8	-0.1	-2.7	3.25
A7B4	17.1	19.6	-2.5	161.5	170.3	8.9	24.2	21.7	2.6	1.2	1.1	-2.9	3.33
B01 17	17.9	17.7	0.2	150.2	150.2	0	245.8	249.4	3.6	0.7	-2.1	0	2.21
B01 14	13.8	15.1	-1.3	167.5	173.7	6.2	200.3	198.9	1.4	-0.58	-1.03	-1.47	1.89
B01 13	15.2	15.2	0	170.5	170.5	0	156.1	148.9	7.2	-1.04	-0.86	-0.02	1.35
B01 10	17.9	18.5	-0.6	149.4	146.5	2.9	108.4	103.1	5.3	-1.68	-0.78	0.24	1.87
B01 08	10.9	10.2	0.7	125.9	125.3	0.6	93.3	94.3	1	-0.08	0.39	0.13	0.42
B02 19	9.7	8.6	1.1	125	127.4	2.4	257.5	266.9	9.4	0.08	-1.38	-0.18	1.39
B02 17	18.2	17.3	0.9	148.8	150.5	1.7	241	247.9	6.9	0.7	-3.25	-0.2	3.33
B02 14	15.1	14.9	0.2	167.1	175.5	8.4	204.1	207.2	3.1	-0.78	-1.71	-0.27	1.90
B02 10	18.4	18.6	-0.2	152.8	146.8	6	99.6	96.1	3.5	-1.76	0.17	1.02	2.04

- the value of standardised bias is within the range expected for data from a normal distribution
- the standardised kurtosis value is within the expected range for data from a normal distribution. So any statistical test with reference to the standard deviation can be performed.

Since data come from a normal distribution (population from which the sample comes can be represented by the normal distribution), the Confidence Intervals can be calculated accordingly. The Confidence Interval for the mean at 95% is [-0.686; 0.277] and the Confidence Interval for the standard deviation at 95% is [0.886; 1.600].

Extrapolating the statistical parameters obtained (Table 5) mineral losses and dilution can be estimated.

By adding or subtracting the mean hole deviations to a blast ring design. the following graphic is obtained (Figure 9). The dilution surface is shown as a light grey colour and the surface due to losses in dark grey.

In this case, the designed cross-sectional area of the ring is 387.0 m^2. while the actual projected area is 358.3 m^2. The net difference of 28.7 m^2 comprises 30.6 m^2 loss (or potential under-break) and 1.9 m^2 of dilution (or potential over-break).

For a burden of 2.45 m and density of 4.2 t/m^3. the potential loss and dilution per blast ring are

approximately 315 tonnes and 20 tonnes respectively. If this potential is fully realised throughout an entire stope this is equivalent to an 8% loss of ore and 0.5% dilution increase solely related to drill hole accuracy (Figure. 10).

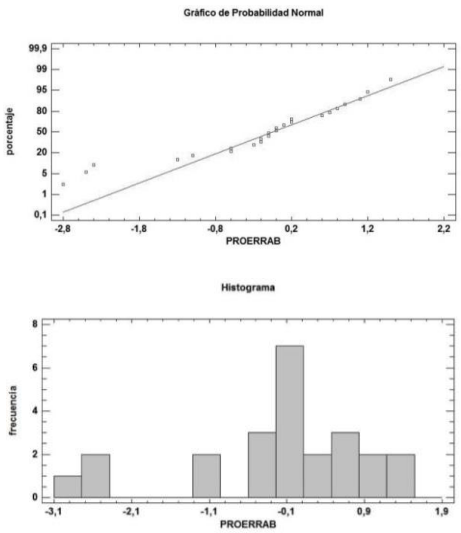

Figure 8. Normal distribution data representation

Table 5. Statistical values for calculations.

Error	Value
Counting	24,00
Average	-0,20
Average (neg)	**-1,02**
Average (pos)	**0,61**
Deviation	1,14
Variation coeficient	-558,92%
Minimum	-2,80
Maximum	1,50
Range	4,30
Standarized bias	-1,83
Standarized Kurtosis	0,48

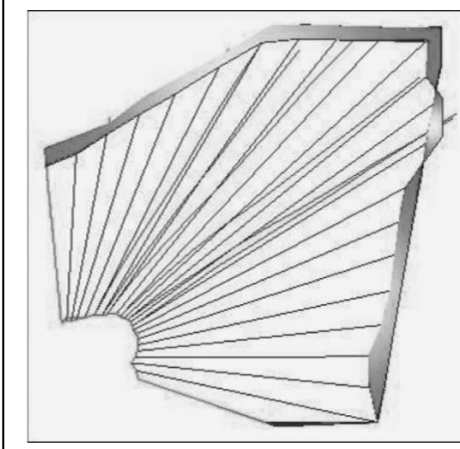

Figure 9. Dilution and loses area modelisation of a ring.

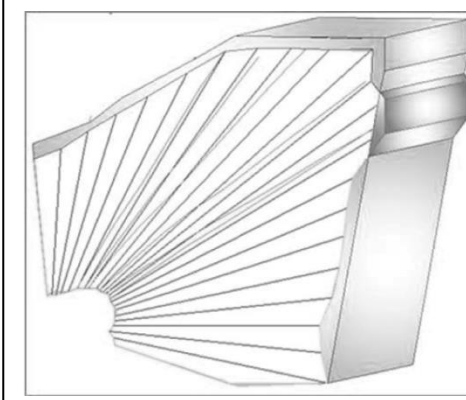

Figure 10. Dilution and loses volume representation in a ring.

5 CONCLUSIONS

The significant potential impact of blast hole accuracy on ore loss and dilution highlights the importance of this kind of study and the need for accurate measuring tools. The automation of the measuring system with minimal interruption to normal operational tasks is a feature of the tool described herein.

This system not only provides useful data for detailed evaluation and potential continuous improvement, but does so in an automatic manner as part of normal charging tasks using existing equipment. This contributes to safety, prompt

results and time savings; all essential attributes of modern mining.

In the mines where this study has been undertaken, a procedure has been established for production blasting. Once the holes have been drilled and before charging, they are cleaned and then measured in order to verify drilling accuracy. With this method, the charging unit is used as an additional element to measure holes so that no time is lost before charging. Unnecessary efforts are avoided and time saved. In addition to these elements, drill design parameters can be modified in order to optimise the procedure and avoid dilution and loss, thus improving operational efficiency.

REFERENCES

Killeen, P.G., Bernius, G.R. & Mwenifumbo. C.J. 1995. Surveying the path of boreholes: a review of orientation methods and experience. Geological Survey of Canada. Natural Resources Canada. Ottawa.

Orpen. J. 2005. Introducing the borehole surveying benchmarking project. Institute of Mine Surveyors of South Africa Colloquium. Voorspoed Mine. Belmont. Republic of South Africa. 5 to 6 May.

Stockholm Conference Proceedings 2017, R. Holmberg et al

A case study to determine of blast efficiency in sub-level caving method via mining software

F.R. Ünal
Istanbul Technical University, Turkey

ABTRACT: The efficiency of drilling and blasting is as important in underground mining as it is in open pit mining. Size distribution of rock fragmentation that occurs upon explosions, impacts the loading, transportation and mineral processing operations' efficiency directly. For blast efficiency analysis, mining software is used more frequently in open pit mining than in underground mining. Blast simulation software used for optimised pre-blast planning and image analysis software used for post-blast rock fragmentations, are the most common mining efficiency software available. Using both of these software is as easy and necessary in underground mining as it is in open pit mining. This study aims to show how and for which purposes mining software applications are useful.

1 INTRODUCTION

Since the mid-17th century, people have been using drill and blast applications for loosening hard rock grounds, applying gun powder as an essential agent. Ever since, drill and blast applications are being used in mining, tunnelling and construction. Aside from being compelled to use drill and blast applications as the only option, people may choose this technique because of its advantages. For instance, drill and blast applications are advantageous because they're flexible, mobile and result in lower capital costs. However, as a downside, these applications require better-qualified manpower to be put into practice. Determining the efficiency of a blast requires various elements to be taken into account such as: rock fragmentation size, blast vibration, blast air/pressure shock, flyrock, the left-over faces conditions. Especially the rock fragmentation size impacts all of the operation levels directly. Fragment size of the blasted rocks should not be coarse because that takes away from the efficiency of mining. Yet fine sizes are not completely desired either. In addition to acquiring an optimal fragment size, keeping up with the initially-intended progress and minimising excessive caving are also crucial measures. Furthermore, the explosives should cost as little as possible.

With this perspective in mind, drilling and blasting operation in Eti Bakır Küre Underground Mining Field, Kastamonu, Turkey has been evaluated. These drilling and blasting operations were performed at gallery driving for generating sub-levels in the ore bed within sub-level caving method. Blast design parameters were carefully measured through extensive evaluations. The parameters of explosives and firing pattern were

recorded in extensive detail together with the shot lengths.

The fastest and the easiest way of analysing rock fragmentation size distribution was using an image analysis software. The key point of taking a proper photograph to analyse was to show the most of the muck pile with two scales. Results of analysis were average fragment size, uniformity index and fine and coarse size fragments.

Also, blast simulations were held using blast design parameters including firing pattern and amount of explosive for each hole. Blasting time contours and energy distributions were obtained. Usage of different type of explosives, such as emulsion explosives instead of ANFO (hydrological circumstances) or less emulsion explosives instead of contour explosives were compared.

2 BLAST DESIGN

In this mining field sub level caving method is applied. This method's requirement can be summarized as big vertical ore bad with hard host rock, which is mostly metalliferous ore deposit. The sub-level caving method works by driving parallel galleries and caving sub-levels between these parallel galleries. In this field both driving galleries and caving sub-levels are done with drill and blast applications at both preparatory and production works. In this study ore face blasts for driving galleries which are part of production works are examined.

2.1 The firing pattern

Olofsson (1988) said that "the main difference between tunnel blasting and bench blasting is that tunnel blasting is done towards one free surface while bench blasting is done towards two or more free surfaces". That's why first blasting holes at face aim to create second free surface regardless of which hole cut system is used, V-cut or parallel hole cut. No more than two thirds of the section width should be targeted as advance under typical conditions (Erkoç 1990). Considering external factors, production goals and rock structure, a suitable pattern was planned for the gallery in ore is 6.70 meters width and 4.70 meters height, and 4 meters hole length for 3.50 meters advance. Hole diameter is 102 mm for relief holes and 48 mm for charge holes; cut holes, roof holes, stopping holes,

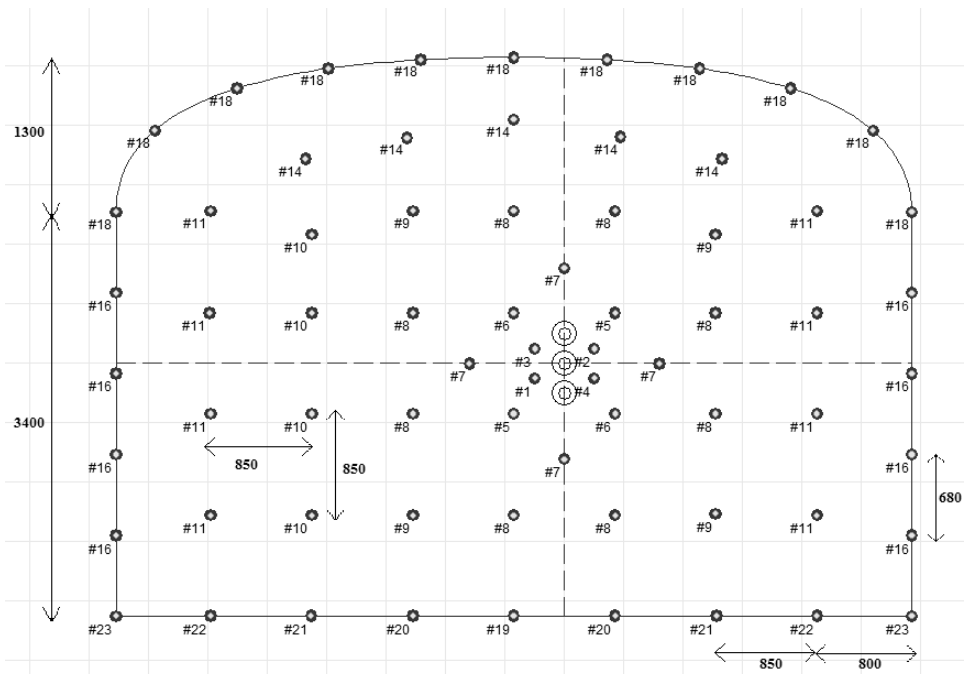

Figure 1. The firing pattern with delay numbers.

wall holes and floor holes.

The firing pattern with hole delay numbers of this field shown in Figure 1. Delay codes (#) and nominal firing times are shown in Table 1. As it can be seen in Figure 1 parallel cut hole technique is preferred with 3 relief holes and 72 production holes. Delay number are #1-23; #1-7 delays are used for cut holes, #16 delays are used for wall holes, #18 delays are used for roof holes and #19-23 delays are used for floor holes.

Table 1. Delay # and nominal firing times.

#	Nominal Firing Time (ms)	#	Nominal Firing Time (ms)
0	0	12	1800
1	100	13	2000
2	200	14	2500
3	300	15	3000
4	400	16	3500
5	500	17	4000
6	600	18	4500
7	800	19	5000
8	1000	20	5500
9	1200	21	6000
10	1400	22	6500
11	1600	23	7000

2.2 Explosive agents

The explosive agents which are used for the pattern shown before are ANFO, emulsion cartridge and contour cartridge. The characteristic properties of these explosives are shown in Table 2.

For production holes, except floor and wall holes, one emulsion cartridge at down the hole and ANFO until 30 cm stemming are used. For wall holes, one emulsion cartridge at down the hole and four emulsion contour cartridges are used for the minimisation of excessive caving. And for floor holes, only eight emulsion cartridges are used because of water inflow at floor holes and ANFO's lack of water resistance. Considering all of these hole contents, charge mass and specific charge per cubic meter can be calculated. Charge mass is 297.28 kg; 36.00 kg from floor holes, 15.84 kg from wall holes and 245.44 kg from other production holes. For specific charge, first volume of blast should be calculated; and it is 120.152 m^3 for 4.00*470*6.70 ore face blast. It is found that the specific charge is 2.47 kg/m^3. But unfortunately these are theoretical calculations. Minimum 3.50 meters advance is accepted. With 3.50 meters advance, the volume is 105.133 m^3 and the specific charge is 2.83 kg/m^3.

3 BLAST SIMULATION SOFTWARE APPLICATIONS

After the blast layout is defined and uploaded to the blast simulation software, including specific

Table 2. Characteristic properties of explosives.

	Velocity of Density VOD (m/sn)	Energy (kj/kg)	Density (g/cm^3)	Heat of detonation (K)	Volume of gases (L/kg)	Dimen-sions of cartridge (mm)	Weight of Cartridge (g)
Emulsion Cartridge	5700	4200	1.16	2852	872	36*420	500
ANFO	4796	3810	0.80	3059	978	-	-
Emulsion Contour Cartridge	5485	2980	1.10	2120	905	19*735	365-375

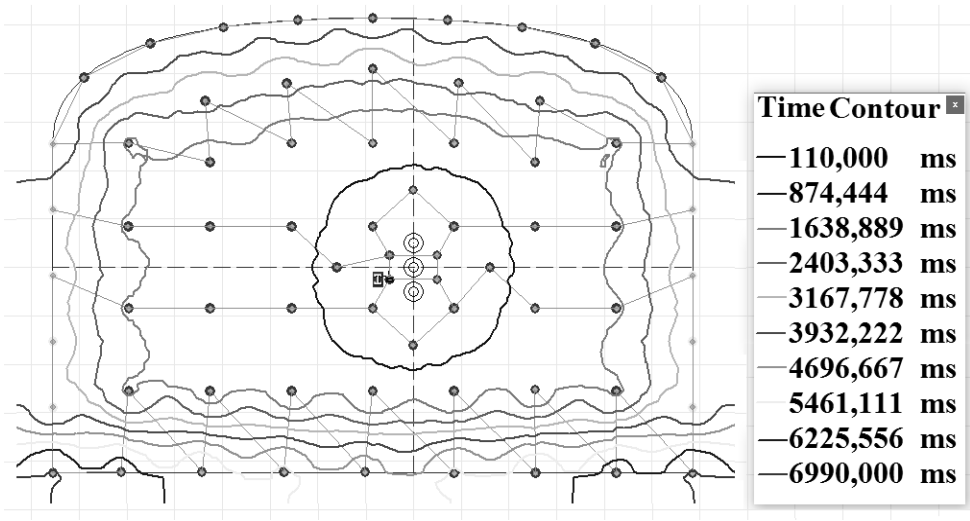

Figure 2. Time contours.

parameters and features of the firing pattern such as explosives, hole features, surface and downhole delays and connectors, blast simulation with the time contours, energy distribution and maximum instantaneously charge outcomes. Time contours are useful to understand whether or not delays and connectors work expediently and pertinent. Detonation timing directly effects energy distribution. It is specifically used to foresee and accurately predict the possible outcomes of excessive caving and fragmentation size. And maximum instantaneously charge is extremely important to efficiency analysis of vibration and sound pick.

3.1 Time contours and instantaneous charge changes

The timing of detonators does not just have impact upon the fragmentation size, additionally upon different results such as excessive caving, vibration, sound and pressure shock waves (Jha 2013). After all necessary data uploaded, time contours outcome as shown in Figure 2.

As shown in Figure 2, first, cut holes are exploded and create free surface to other holes to explode. And last, corner floor holes are explode as expected. With these time contours, it is clearly seen that delays are optimal and in order. Every hole has their own free space which us created by holes exploding before.

Instantaneous charges are important as mentioned previously and it is the software's other output (Figure 3). The maximum instantaneous charge is 51.92 kg at 4500 ms which is delay #18. There are all 11 roof holes explode with delay #18. The second maximum instantaneous charge is 37.76 kg at 1000 ms and 1600 ms which are delay #8 and delay #11. There are 8 holes at each delay.

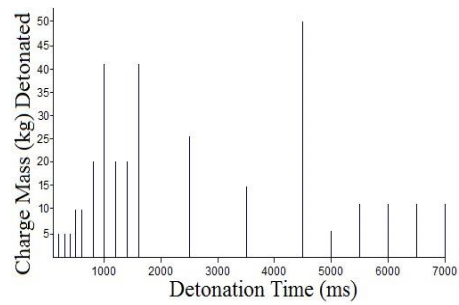

Figure 3. Charge mass (kg) detonated vs. detonation time (ms).

Also instantaneous number of decks detonated vs. detonation time graph is shown in Figure 4, and there are three different delay columns which have second maximum instantaneous number of decks detonated. Not only delay #8 and delay #11 but also delay #16 has same number of decks detonated. But delay #16 does not have the second

maximum instantaneous charge. The reason is the holes are wall holes and to prevent excessive caving, there are lesser explosives in them than other charge holes.

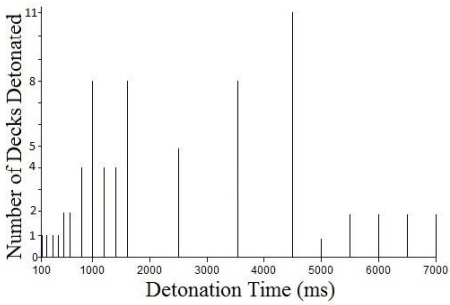

Figure 4. Instantaneous number of decks detonated vs. detonation time (ms).

3.2 Energy distribution analysis

An energy distribution of a blast pattern shows where explosives are less or more than it should be. If it is less, there would not be enough fragmentation. And also more explosive is not required to prevent fine sized particles, excessive caving and cost. That's why the amount of explosive should be optimal. The energy distribution of this firing pattern is shown in the Figure 5. As shown and expected highest energy occurs around cut holes and the least energy occurs around wall holes. It is observed that using emulsion contour cartridges to prevent excessive caving works and creates less energy. According to the energy distribution graphic, it can be assumed that fine sized fragments come from around cut holes, and coarse sized fragments come from around wall holes.

4 IMAGE ANALYSIS SOFTWARE APPLICATIONS FOR FRAGMANTATION

In recent years, image analysis software has been used, especially at open pit mining for fragmentation efficiency analysis. Image analysis software is more efficient and practical. Multiple images can be analysed rapidly and there is no need to stop production (Maerz *et al.* 1996). For example, at open pit mine, all of a pile cannot be graded and screened to size separation. But with an image of all of a pile, size distribution can be found. The difficulty of having appropriate image at underground mine, is lack of light. Artificial lights such as powerful flashlights, portable searchlights and even headlights of a truck or a dredger, can be enough. These artificial lights should be used carefully because for appropriate image, shadows and contrast are very important. Another critical issue is using two objects as a scale. Same as at open pit mines, piles have slopes,

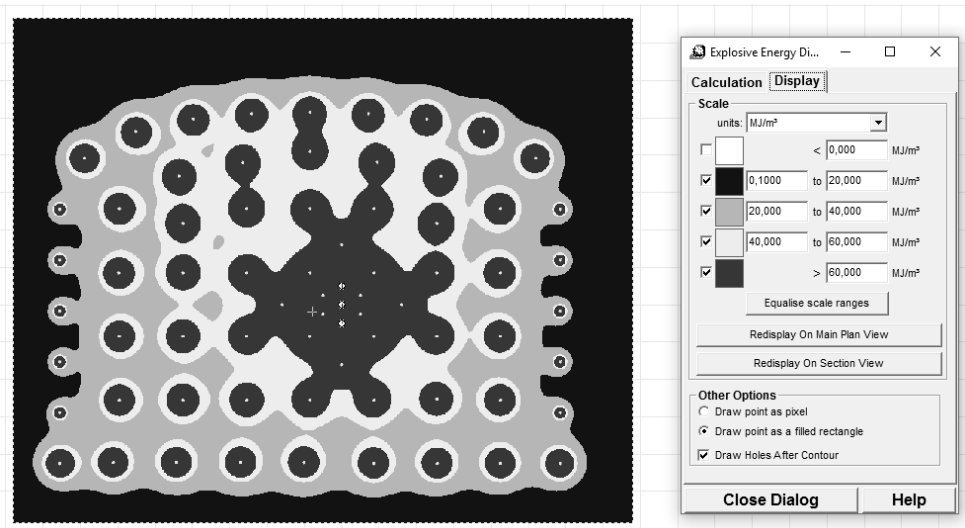

Figure 5. Energy distribution of blast.

that's why there should be two objects as a scale to make software comprehend perspective of pile. Objects can be anything; empty boxes of explosives, regular scales or plastic plates, as long as dimensions of the objects are known.

Outputs of image analysis software are granulation histogram and granulation curve, data tables, including cumulative particle size table, analysis of particle count and statistics, percent passing sizes as characteristic percentile sizes, average particle sphericity (WipWare 2013). Each of these data gives different information about blast and fragmentation efficiency.

4.1 Preparing the image for analysis

Having an appropriate image is crucial. After uploading image to software, there are processes should be done manually.

First, image should be cropped if there is useless space; too dark, too light, shadowy or space without particles. Two images are shown in Figures 6 and 7 as an example of an original appropriate image and a cropped version of it. And then the software creates a net which sets boundaries of particles. This net can be improved manually by the user but it is not necessary for all net and image pairs.

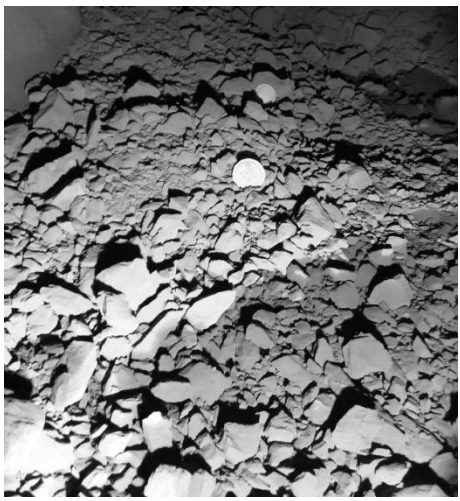

Figure 6. The example of the original appropriate image.

The image with net is colourized by software to make it easy to understand particle sizes and whether or not net is accurate. The colourized version of cropped image (Figure 7) is shown in Figure 8. The accurate net and the image can be turned into the output as analysis results by software.

Figure 7. The example of the cropped version of the original appropriate image.

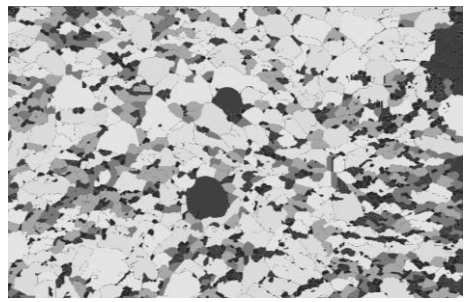

Figure 8. The colorized version of cropped image

4.2 The Analysis Results

After the software runs with image prepared, it only takes a few seconds to be analysed. The analysis results of the image (Figures 7 and 8) are shown in Figure 9.

The data table shown on the left side, includes statistical numerical data; minimum and maximum particle sizes, mean value, standard deviation.

Also, there are passing sizes for different percentages, and they are characteristic percentile sizes. It was clearly explained as 'D10 is the ten-percentile, the value for which 10% of the sample is finer and 90% coarser; in terms of sieving, D10 is the size of sieve opening through which 10% of the sample would pass," (Sanchidrian & Singh 2013). In summary, D10 specifies the state of fine sized particles. Likewise,

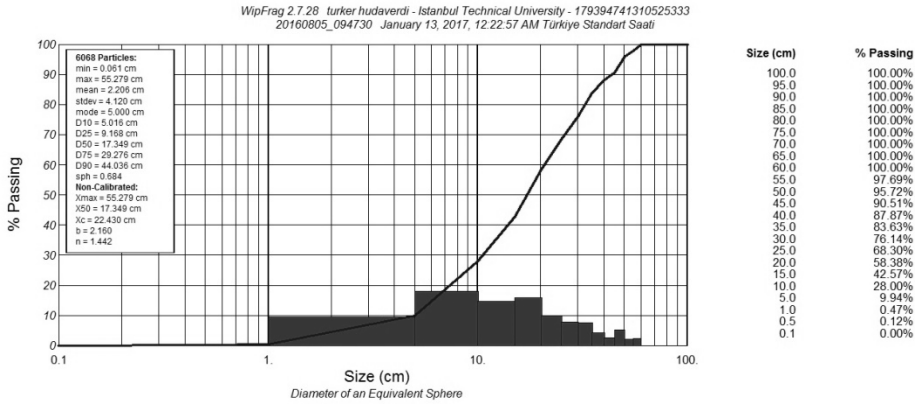

Figure 9. Results of analysis.

D50 represents the state of mean sized particles and D90 represents the state of coarse sized particles.

The histogram shows granulation and the curve is cumulative percent passing curve. The cumulative particle size table shown in the figure on the right side, is table state of the curve.

The uniformity index is a measurement unit which shows how consistent particles sizes are. The greater the uniformity index, particles are closer in size.

For seven different blasts, after blast fragmentation image analyses were performed. The blasts features are shown in the Table 3.

Table 3. The features of analysed blasts.

	1	2	3	4	5	6	7
Emulsion Cartridge (kg)	80	70	80	220	70	80	60
ANFO (kg)	200	225	225	0	225	200	175
Emulsion Contour Cartridge (kg)	10	10	10	10	10	10	10
∑ (kg)	290	305	315	230	305	290	245
Number of Decks	71	72	79	68	72	68	60
Advance (m)	3.80	3.40	3.20	3.80	3.40	3.60	3.70

Characteristic percentile sizes, D10, D50 and D90 of the seven blasts analysed shown in the Figure 10. D10 and D50 results are consistent, even though D90s are not. This can be due to many variables, mostly from discontinuities which cause energy loses.

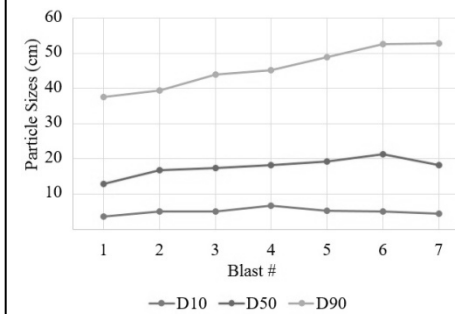

Figure 10. Characteristic percentile sizes D10 D50 D90.

For D50, the average value is 17.72 cm, the maximum value is 21.34 cm at the sixth blast and the minimum value is 12.89 cm at the first blast. For D10, the average value is 5.05 cm, the maximum value is 6.70 cm at the fourth blast and the minimum value is 3.71 cm at the first blast. As a conclusion of these results, it can be said that D10 and D50 results are steady and compatible with each other. On the other hand, D90 is not. For D90, the average value is 45.81cm, the maximum value is 52.84 cm at the seventh blast

and the minimum value is 37.59 cm at the first blast.

Even if the particle sizes for seven blasts' analysis look consistent with each other, for the consistency in each blast, uniformity index should be looked at (see Figure 11). As mentioned before, the uniformity index is a measurement unit which shows how consistent particles sizes are. The greater the uniformity index, particles are closer in size. Mathematically, it is the slope of a cumulative percent passing curve.

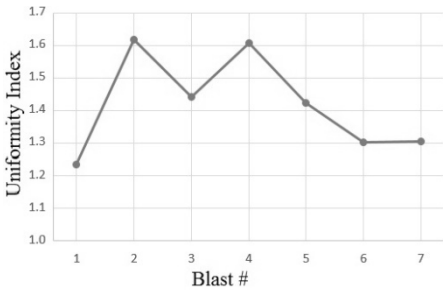

Figure 11. Uniformity index results.

The fragmented particles from the first blast seem closest to one another in the terms of characteristic percentile sizes, not in terms of uniformity index. In fact first blast fragmentation uniformity is least according to uniformity index; even it is within acceptable range. Although the results may vary depending on the operational technique, uniformity index above 1.00 are considered plausible and those that exceed 1.50 are successful.

Each one of the analysis results of image analysis software can be specifically useful for different operational optimisations. Characteristic percentile sizes are used to determine optimal amount of used explosives. Uniformity index examines the compability of fragmentation with continuity of efficient post-blast operations.

5 CONCLUSION

Essentially the aim of this study is to show that the mining software need not be exclusively used in open pit mining but can be used in underground mining with ease, as well. When using the simulation blast software, creating firing patterns takes more time in underground mining than it does in open pit mining due to the use of face pattern which requires a little more specialised treatment of the holes. The holes require to be placed by hand and different types of explosives may be needed so that the necessary accommodations to cases of excessive caving and inflow of water, are made. The critical step in using the image analysis software is to make sure that one uses the appropriate image. To make that possible, one should make sure that the image contains two objects for scaling purposes and is shot under appropriate lighting. As long as the proper image is used, the software works the same as it does in open pit mining.

In the realm of mining, conventional practices should be replaced by those that are in line with the fast-pace of technological discoveries and consequently are more efficient, practical and convenient. Failure to use and make the best of these latest practices results in regressions in the field of mining in the grand scheme of things and therefore should be highly avoided. With regard to this approach, using mining software in underground mining should be highly encouraged.

REFERENCES

Erkoç, Ö.Y. 1990. *Kaya Patlatma Tekniği.* İstanbul: Çelikler.

Jha, A.K. 2013. *Evaluation of mine productivity and economics by effective blast instrumentation—A techno economic proposition.* Ranchi: David Publishing.

Maerz, N.H. 1996. *WipFrag Image Based Granulometry System.* Rotterdam: CRC Press.

Olofsson, S.O. 1988. *Applied explosivestTechnology for construction and mining.* ARLA: Applex.

Sanchidrian, J.A. & Singh, A.K. 2013. *Measurement and analysis of blast fragmentation.* Boca Raton: CRC Press.

WipWare. (2013). *Sampling and analysis guide.* Ontario: WipWare Inc.

Stockholm Conference Proceedings 2017, R. Holmberg et al

A new era of blast initiation systems reducing safety risks, costs and enabling automation

B. Wicks
Orica Europe, Troisdorf, North Rhein Westfalia, Germany

M. Lovitt
Orica Australia, Subiaco, Western Australia, Australia

ABSTRACT: This paper will discuss the history and development of wireless blasting, describe the verification, and validation performed and introduce the advantages of the next generation of blasting to the market; including safety, cost and automation.

1 HISTORICAL

The first known commercial interest in wireless initiation, found in the literature by the author, was in 1945 and authored by Imperial Chemical Industries, previously a parent company to Orica. The early patent describes a control system for detonating a charge, which upon reception of multiple wireless signals initiates said charge.

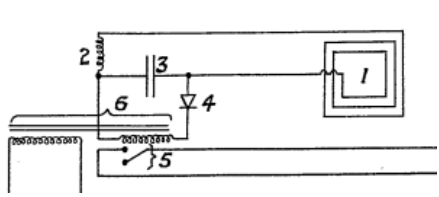

Figure 1. An image illustrating the wireless receiver from an early patent for a directly initiated detonator.

Further progression of wireless blasting and the development of a commercial wireless initiation system received only limited interest until recently, when remote blasting capability was developed and in 2003 commercialised. In such a remote blasting system, the blast is controlled from a remote location by 2-way radio communication with the in-hole primers connected by wire to radio transceivers on surface. This is the predominant wireless initiation system used in mining systems today.

Orica has been developing WebGen™100 for over a decade; a more advanced, true wireless system, capable of directly initiating in-hole primers via one-way communications that penetrates rock, water and air. This system is the first commercial initiation system to incorporate the initiation energy and ability to initiate completely within the device. To achieve this fundamental change significant investment and an

evolution of the functional safety and design of initiation systems was required with substantial increase in verification and validation activities.

Figure 2. Evolution in the design of the directly initiated wireless booster.

The prototypes generated during the development of the wireless booster are shown in Figure 2. The initial prototype design was a comparatively larger cylindrical device focusing on larger surface boreholes and, as the development matured, the design was refined and reduced through a number of iterations. The final design was chosen as its size and performance affords the ability to target the majority of blasting applications.

2 INTRODUCTION TO SYSTEM

The wireless system consists of three different categories of components; the blast management computer; the wireless in-hole primers, encoder controller and accessories; and the transmission system; shown in Figure 3.

Prior to introducing wireless blasting to a mine site a wireless survey is conducted. The survey qualifies the suitability and performance of the wireless system at the site. The information from the survey is used to identify a suitable location for the transmitter, recommend a preferred antenna to be used; identify any anomalies, which may significantly attenuate the signal; and sources of noise, which may interfere with the signal.

As per current practice, the blast is initially designed with blast design software such as SHOTPlus™. The blast design is then exported to the blast dongle and loaded into the Code Management Computer (CMC); a dedicated tablet PC that hosts and manages blast codes for a blast site. Each set of codes consists of a blast group identifier, mine specific identifier and firing codes

① Booster
② PlugIn detonator
③ Disposable receiver (DRX)
④ Encoder Controller with attachment
⑤ Transmitter Controller
⑥ Transmitter and battery pack
⑦ Quad loop antenna
⑧ Code Management Computer (CMC)

Figure 3. WebGen™ 100 blasting system.

specific to each blast and is required to initiate the blast.

The wireless in-hole primer consists of a disposable receiver (DRX), a booster and detonator. Prior to encoding the detonator and DRX are mated energising the assembly. To encode the assembly, the Encoder Controller, a hand-held device connected to an encoder cradle is used. The assembly is placed into the cradle where communication of required blast parameters and interrogation of the unit are performed. The performance of the DRX and detonator are then evaluated and verified, encoded with the blast codes, and the timing and the detonator are recorded. Finally, the detonator, DRX, booster and components are assembled at the loading bench to create the primer, before being loaded into the required position.

The transmission system creates the electromagnetic signals that enable firing of the wireless primer. During the blasting sequence, the user controls the transmitter via transmitter controller. The system supports a short-range and long-range antenna, either a quad-loop or cable-loop type. The user enters the fire command into the transmitter controller, enabling the firing signal to be sent via transmitter to all corresponding primers in range.

During the trials, the long-range cable-loop antenna was deployed. The radiation pattern for the antenna is shown in Figure 4. The specified range of this antenna, when operating in a standard environment confirmed by a survey, is 720 m in the vertical direction and 800 m in the horizontal plane.

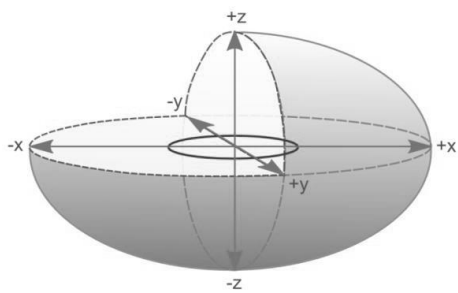

Figure 4. Transmission range of system.

3 INCREASED SAFETY THROUGH REDUCED OR ELIMINATED RISKS

There are so many mining methods to recover ore from underground and they all rely on the basic premise to break the ore into a manageable fragmentation size for extraction and then to stabilise the resultant void with fill material. The breakage of the ore spans from ‘drill and blast’ to using the stresses of the void to break ore to enlarge the void, as in block caving. Practically all hard rock mining requires the drill and blast process for a large part of the setup or production stages.

Blasting is, by its nature a cyclic process that requires digging, drilling and blasting processes. The digging and drilling processes have been principally controlled with large-scale equipment that allows automation or the operator to be protected in a cabin where the conditions can be controlled. The blasting process, while options to automate the charging exists, has always required a very manual approach to the connection of the blast to a firing system and in most methods this occurs in the area of highest potential risk of injury due to rockfall and or unstable workplace due to movement of the floor.

3.1 Sub-level cave

Underground production blasting requires a level of exposure to situations of increased risk. This is especially apparent during connection of the wire network of the initiation system. Sub-Level Caving (SLC) operations in particular require this hook up within close proximity to the edge of the excavation and commonly above a bank of rock prone to movement. A number of SLC mines have had rushes that have resulted in fatalities in recent years.

Orica’s Wireless Electronic Blasting System eliminates these high-risk hook-up processes and facilitates the development of automated charging. The system enables blasting techniques whereby in-hole primers initiate directly by communication though rock without the requirements of physical connections. Elimination of the wire network and connectors removes the need to have access to the collar of the hole after charging. This enables increased pre-charging of underground blast patterns, whereby a larger number of holes are initially charged, and the flexibility to initiate a group in each blast event.

SLC mines have situations where the edge of the excavation has retreated, or broken back, past the next ring to be blasted. If this occurs, either the next ring is fired, wasting primary draw and causing potential bridges/oversize, or re-drilling is required in these locations. Having an operator

Figure 5. Underground vehicle at SLC mine after an inflow.

Figure 6. Hook-up for a single SLC ring with risks partially controlled with backfill, shotcrete and bunding.

Figure 7. Multiple wireless charged rings are ready to fire as soon as needed, note strapping indicators.

re-enter these areas and re-drill is both a costly exercise, and an activity with higher safety risk and slowing productivity.

The loading procedure for wireless initiation uses packing tape that hangs out of the bottom of the hole to indicate that the ring has been charged, and as an indicator for the loader operator to determine if the charges have been moved by ground pressure of earlier fired rings. Further details of production blasts are found in Liu *et al.*

There are many papers and case studies, including S.Steffen *et al.*, that show that having the primers in the correct place and reliable initiation; will improve primary recovery and minimise dilution. Wireless will enable every blast to be reliably initiated; with electronic timing, the blasting sequence for the near-optimal fragmentation can be achieved.

3.2 Sub-level open stoping

Sublevel Open Stoping (SLOS) has exposures due to the open stope. Ground within the open stope is normally not supported and uncontrolled falls of rock can be expected, which is why they have barriers to protect personnel entry. Mines use bunding and other means to protect potential falling rock into the work area, but the edge of the next blast packet requires charging and hooking up for the start of the next blast. Furthermore, where stress and ground conditions create unstable or squeezing conditions, the next blast can be delayed due to blast hole closure or dislocation.

This is a major delay cost and a heightened safety risk to control in recovering, re-drilling and correcting before charging can be undertaken.

Wireless allows the next blast section to be loaded and pre-charged before the previous section is fired, thereby eliminating the influence of dislocated and squeezing holes, and the high-risk process close to an open stope, on the charging process. Obviously, the priming frequency should, as it is now, be chosen to allow for primers to initiate the most of the explosive charge in the blast hole. The type of initiation does not change the frequency and position of primers in a blast hole. The frequency is decided from the level of discontinuities in the rock, the powder factor in the blast and the criticality of the blast hole.

Another example of this use is in an opportunity to leave isolated pillars to improve the stability of Open Stopes and the recovery of ore by leaving these pillars behind in the centre of a stope after it has been charged with the wireless initiated explosives. This method can increase the size of stopes and reduces the frequency of slots. It increases the recovery of the ore body and reduces costs. Extra support from these pillars can assist the clean ore recovery before the isolated pillar is extracted.

3.3 Seismically Active Mines

Further difficulties may arise within mine locations prone to seismic events. These active

Figure 8. Charging complete for the hook-up process to tie it into the detonating cord at the open stope brow.

areas require further management controls including exclusion zones to limit the exposure of personnel to rock bursts and closures. Traditional blasting methods in these areas will require an operator to access the hazardous area and hook up the initiation system prior to blasting. An example would be a block cave mine which is newly establishing the cave or due to high stresses on the Undercut Level. Pre-loading several rings away from the high stress 'active' areas can mean that these areas can be remotely dug and fired when wireless initiation systems are used.

The wireless system is uniquely suited to this use as the detonator complex can be made up and loaded into a cassette for use in an autonomous charging vehicle capable of making up the primers, inserting them into the blasthole (either up or down) and charging.

4 SYSTEM VALIDATION AND VERIFICATION

Wireless Electronic Blasting technology is being introduced into production environments following the successful product development and verification stages. During these stages, the system validation was performed by leading internal experts and external authorities; in laboratory, underground and surface operating environments.

The five stages of testing performed on the system are described in this section; consisting of System Lab Tests performed during development; Internal Field Trials, Customer Trials, Live Trials and Production Trials performed during the final system tests in the first half of 2015.

4.1 System lab validation and verification

Orica teams located in Troisdorf, Germany, and Brownsburg, Canada, and five independent external organisations located in Germany, Canada and the USA performed the design and lab testing. The external organisations included our design, functional safety and independent lab verification partners. A summary of the battery of validation and verification tests performing on the system in order of ascending system design level is included below.

Firmware, module, and unit testing, verified and validated the smallest individual testable blocks of the system, and was performed both internally and by the project design consultant, and included complete code coverage testing of the firmware, individual module and unit testing via both software and interfacing with hardware firmware.

Design, integration and system tests were

Figure 9. Early remote-control charging equipment with smart vision systems to identify blastholes.

performed to verify that the integration of the software and hardware tested modules performed as specified. As the lower level functionality has previously been tested a 'black box' testing methodology against the system requirements was performed.

Figure 10. System testing of wireless units.

Fault-Insertion testing was performed by both our functional safety partners and by ourselves. Within this testing regime, faults were injected into the firmware and hardware of the device to increase the coverage area and investigate the robustness of the system. The injected faults were triggered by modified source code and via external electrical stimulus.

Finally, assembly and finished device testing were performed on the finished device aiming to provide the best possible test coverage by only exercising the functionality present in the device. Qualification testing was also performed on the finished device, including water ingress, dynamic shock, and electro-static discharge performed by external certified authorities to assess the product for introduction to market.

In total, more than 240,000 tests were performed during the verification and validation of the system. A summary of the overall documented number of tests performed at each stage of verification and validation is shown in Table 1.

4.2 Internal field trials

Wireless internal field-testing trials occurred at Orica Kurri Kurri Technical Centre near Newcastle, Australia, throughout January 2015. The trials involved further functional verification of the entire system in a field environment and also included feedback for the refinement of the design. Measurements were taken across a large forested geographical area with only limited infrastructure. Within the 2,500-meter radius of the trial environment the infrastructure included an emulsion plant, explosive testing ground,

Table 1. System lab validation and verification of system.

Stage	Number of Unique Tests	Number of Times Performed	Total Tests Performed
Firmware, Module, Unit	104	>1,145	119,080
Design	47	>4	188
Integration	17	>3	51
System	169	>3	507
Fault-Insertion	28	1	28
Assembly	5	>1,000	5,000
Finished Device	22	5,303	116,666
External Lab	3	1	3
Qualification	22	1	22
Shock and Dynamic Shock	18	40	720
Pentex™ W Booster	12	135	1,620
Accessories	4	20	80
Totals	>>450	-	>>240,000

Figure 11a. Lab testing of wireless units.

magazines, workshops and a number of commercial office buildings. The system was initially validated with dummy explosives with the range of the devices starting at 300m and increasing gradually to 2,500m. It was verified that system performed as expected, successfully receiving the signal to a range of 1,650 meters. A number of further test were performed at longer ranges between 2,000 and 2,500 meters, but no signal was received at these distances. A summary of the testing and figures are shown in Table 2.

4.3 Customer trials

Initial trials on customer sites were conducted at a customer range in NSW, Australia, during January and February 2015. The aim of the trials were to gain further understanding and data of the field performance of the system, and to introduce the wireless boosters to boreholes loaded with bulk.

Figure 11b. Lab testing of wireless units.

Table 2. Summary of internal field trials.

Range (m)	Number of Trials	Number Units	Number Fired	Percentage	Notes
300 - 1650	15	386	386	100%	Dummies
2000 - 2500	2	30	0	0%	Dummies
500	1	2	2	100%	Detonators

Figure 12a. Orica internal testing of wireless units.

Figure 12b. Orica internal testing of wireless units.

Figure 12c. Orica internal testing of wireless units.

The customer site was a quarry adjacent to a cleared field with limited surrounding Infrastructure, outside of the crusher and engineering workshop. The firing range used during the customer trials was limited to approximately 600 meters due to the geology and size of the site. The transmitter was deployed near the boundary fence and a pattern of boreholes was drilled at the opposite boundary of the site.

During the initial week of the trial, dummy units placed on the surface to confirm the system was deployed and functioning correctly. Once the system was validated the units were positioned in the base of the blastholes and again verified.

During the final week of the trial, live explosives were introduced to the site. The initiation chain was increased in steps; initially, the trials were simulated with dummy explosives, and after successfully simulating the trial, detonators, then boosters and finally bulk explosives were introduced.

4.4 Production trials

Following the successful lab, field and customer site testing the wireless system was introduced to a customer's production blasting. The introduction occurred at a different customer quarry site from the previous tests, though also in NSW, Australia, during February 2015.

Table 3. Summary of customer field trials

Range (m)	Number of Trials	Number Units	Number Fired	Percentage	Notes
500	21	204	204	100%	Surface Dummies
500	21	110	110	100%	In-Hole Dummies
570	5	40	40	100%	Dummy
500	4	9	9	100%	Boosters
555	1	8	8	100%	Bulk
500	1	2	2	100%	Bulk

Figure 13. Customer field-testing of wireless units.

Table 4. Summary of production trials.

Distance (m)	Number of Trials	Number Units	Number Fired	Percentage	Notes
450	4	104	104	100%	Dummy
450	3	32	32	100%	Production
400	1	88	88	100%	Production

A simulated blast was initially performed to ensure the functionality and correct setup of the system which was successful. For the production blasts, blast holes were double primed with wireless units at the top and bottom of the holes. A number of smaller limited production shots were initiated to gauge the performance differences between wireless and i-kon blasting.

As all previous blasts were successful, the final larger production blast, of 88 wireless units, was initiated. All units performed as expected and the blast initiated as designed. Images and details of the blast results are presented in Table 4.

5 SUMMARY AND CONCLUSIONS

This is an introductory paper and a precursor to a number of further production trials. Some of the actual and potential applications, details of the testing and preliminary results of introductory

Figure 14a. Production testing of wireless units.

Figure 14b. Production testing of wireless units.

production trials in operational mines are presented.

6 ACKNOWLEDGEMENTS

The authors wish to acknowledge their gratitude to the following colleagues for their assistance and support throughout the wireless development and trials including: Orica Brownsburg Technical Centre, Canada, including Dawn Goosen, Daniel Mallette, Francois Guillemette, Yves Hamel, Pascal Durand, Marc F Green, Gabriel Gaudreau; Orica Kurri Kurri Technical Centre, Australia, research team, including Richard Goodridge, Johann Zank, Matthew Craft, Maciej Ciez, Tuan Nguyen, Emma Cook, Geoff Stevenson, Laurie Simpson; Orica Troisdorf Technical Center, Germany, including, Dirk Hummel, Thomas Boos, Christian Juenger, Jan Lindenau, Walter Piel, Margit Fischer-Michely, Ulrich Steiner; Orica Gyttorp Technical Center, Sweden, including Johan Lind; and our external consultants from Germany, Canada, and the United States.

REFERENCES

Orica. *WebGen™100 User Manual*. Orica.

AusIMM Underground Operators conference in Australia in October 2017.

Liu, Z., te Kloot, C., Purvis, T., Thomson, S. & Lovitt, M. Improving safety through technology: Orica wireless electronic blasting system trials at Ernest Henry mine. *13th AusIMM Underground Operators' Conference, Paper Number: 30*.

Steffen, S. & Kuiper, P. 2014. Case study: Improving SLC recovery by measuring ore flow. *Caving* 2014.

Stockholm Conference Proceedings 2017, R. Holmberg et al

Influence of stemming length and initiation sequence on rock movement and dilution during a blast

M. Lachamp & R. Chavez
EPC Groupe, 61 Rue Galilée, 75008 Paris, FRANCE

S. Grannas
Mandalay Resources Corporation, 76 Richmond Street East, Suite 330 Toronto, CANADA

ABSTRACT: Björkdal is an open pit and underground gold mine located in northern Sweden. The study briefly presented in this paper has been carried out in the open pit part of the mine. In this mine, the ore body is an assembly of vertical quartz veins, with a thickness varying between a few centimetres and two metres. This disposition in vertical veins makes the ore very located among vast zones of waste. In this context, movements linked to blasting have an impact on selectivity. The goal of the study was to increase the knowledge of how the rock moves during a blast so we could implement it into the design parameters and improve the outcome, such as less dilution and rock movement. Here, we focused our interest on what kind of pre-blast and post-blast information could be measured and what kind of correlations could be assessed from such information. The measurement techniques deployed to carry out this study included drones for generating a 3-D modelling of pre and post-blast areas; modelling from which we extracted swelling fields to assess the muckpile shape. We also used the information from drilling reports to estimate, hole by hole, the top layer's fragmentation from the previous blast. At this time, we also updated the Expertir software to directly import data from rigs and calculate the most efficient stemming for each hole in the blast pattern. The rock movement during the blast was recorded by BMM® sensors placed at different locations and on three different layers in the blast area. We carried out some tests with different initial parameters in the blast design and, from all the records, highlighted correlations between stemming blown out, swelling and local rock fragmentation. We also found an interesting way to improve the rock movement by adapting the stemming, hole by hole, to the surface fragmentation from the previous blast. That's what we propose to show during our presentation: techniques of pre and post-blast measurement, and our first results and ways of improvement concerning the reduction of dilution during blasting.

1 RECORDED DATA AND PROTOCOLS OF MEASUREMENTS

For each test blast, we aimed for measuring the following parameters:

- average rock swelling
- standard deviation of the rock swelling
- horizontal rock movement
- upper layer fragmentation induced by the previous blast

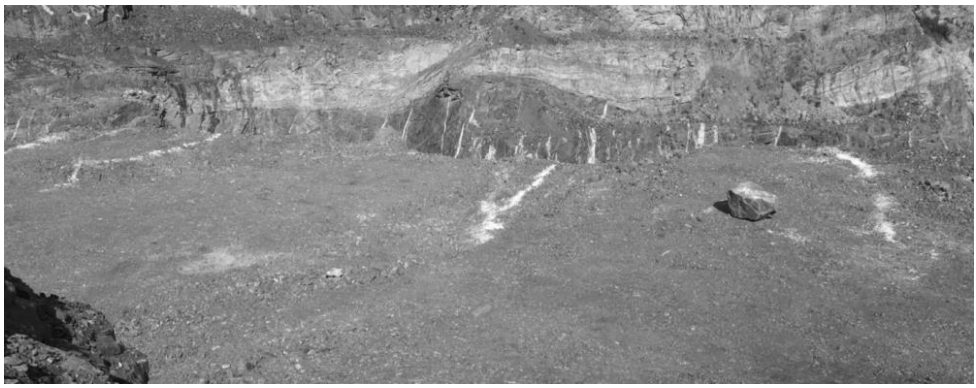

Figure 1. Quartz veins (in white) viewed from the top of a bench.

– rock fragmentation after the blast

Blasts parameters like hole pattern, charges used and initiation sequence were saved for each blast in the Expertir software. Expertir is a blast design software internally developed by EPC Groupe. More qualitative information such as photos, videos of each blast and excavating operator's feedback were also recorded.

For measuring the rock swelling we used a drone carrying a camera. It allowed us to recreate a 3-D model of the blasted area by photogrammetry. For each blast two models were created: one before the blast and one after the blast. Each model was geo-referenced. By comparison of both models in CloudCompare (open source software for 3-D point cloud processing) software towards the vertical axis, we have been able to evaluate the swelling and the muckpile shape.

In Figure 2, the highest areas are displayed in dark grey and the lowest ones in black. The Gaussian distribution of elevations within the muckpile can also be displayed and gives us information on how even the swelling was (Figure 3).

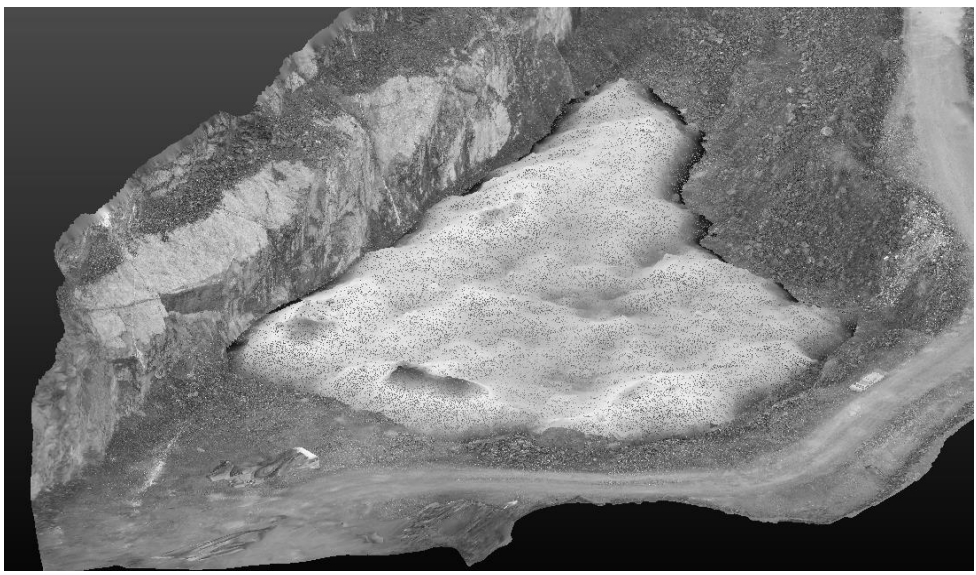

Figure 2. Swelling field displayed on the 3-D model created before blasting. (Blast N°110b3003).

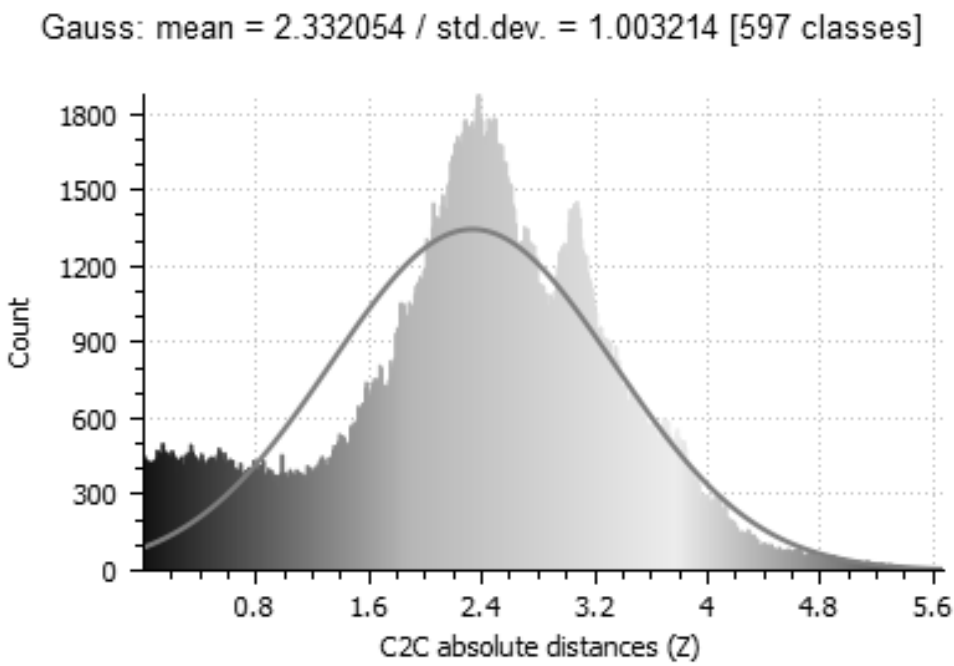

Figure 3. Repartition of elevations within the swelling field with its mean and standard deviation in metres (Blast N°110b3003).

The horizontal movement was measured by BMM® sensors. BMM® sensors are directional transmitters installed in dedicated blast holes. By measuring the position of these sensors before and after the blast, it's possible to find the vector of displacement in different areas. For economical reasons, BMM® sensors were only used in blasts containing ore. The number of BMM® sensors used was different for each blast, depending mainly on the number of veins and their repartition. The sensors were dispatched at the rate of 3 sensors per monitoring hole as shown in Figure 4.

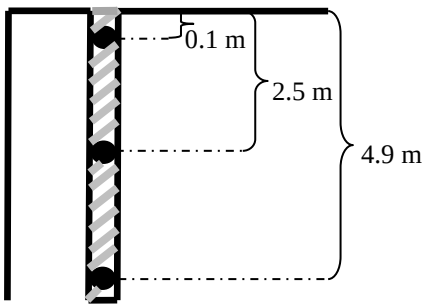

Figure 4. Loading pattern of a 5.5 m deep monitoring hole.

From the movement recorded by BMM® sensors, the mine is able to create the polygons marking the ore's new position; and this for each layer. For the project, the mine also transmitted those polygons to EPC to display them in Expertir on the blast plan. By superposition of these polygons and the initiation sequence in Expertir, we have been able to correlate the horizontal movement with the sequence.

For measuring the rock fragmentation before the blast, we used the penetration rate provided by drilling rigs in IREDES files (Figure 5). IREDES is an abbreviation for International Rock Excavation Data Exchange Standard. It is an industry standard for the data exchange format.

Imported in Expertir for analysis, this penetration rate gave us an estimation of the depth of the rock fractured by the previous blast, and this for each hole (Figure 6).

As can be seen in Figure 6, the quality of the rock varies a lot from one hole to another. The rock fragmentation after the blast was evaluated in

```
<start_time>2010-05-21T17:30:22.050Z</start_time>
<stop_time>2010-05-21T17:37:52.126Z</stop_time>
<azimuth>24.06773120</azimuth>
<dip>0.74003105</dip>
<start_at_collar>true</start_at_collar>
<collar>
    <northing>316.38344036</northing>
    <easting>2159.03635791</easting>
    <elevation>-109.34431231</elevation>
</collar>
<length>6.16400000</length>
<penetration>
    <tag_time>2010-05-21T17:30:27.182Z</tag_time>
    <length>0.30400000</length>
    <rate>0.07596202</rate>
</penetration>
<penetration>
    <tag_time>2010-05-21T17:30:31.176Z</tag_time>
    <length>0.37100000</length>
    <rate>0.01674581</rate>
</penetration>
<penetration>
    <tag_time>2010-05-21T17:30:35.372Z</tag_time>
    <length>0.41000000</length>
    <rate>0.00928129</rate>
</penetration>
<penetration>
    <tag_time>2010-05-21T17:30:39.382Z</tag_time>
    <length>0.45100000</length>
    <rate>0.01023976</rate>
</penetration>
```

Figure 5. Structure of IREDES file extracted from drilling rigs.

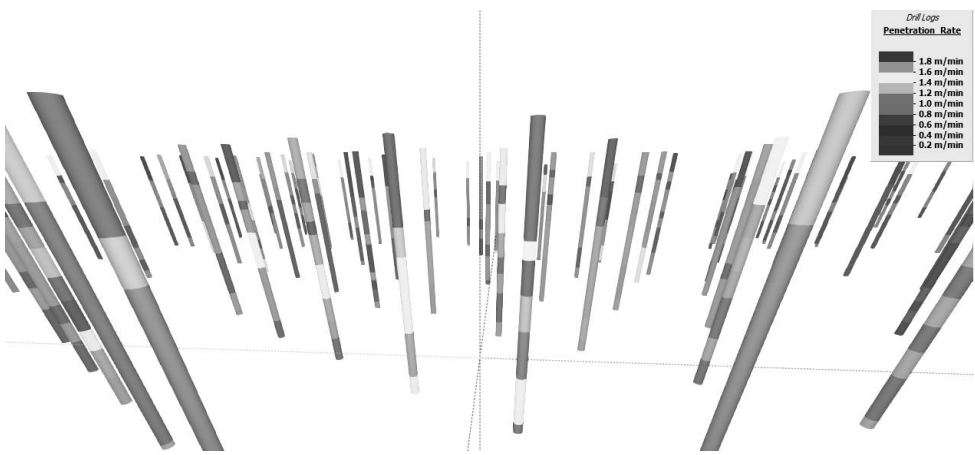

Figure 6. Display of penetration rate for each hole in Expertir.

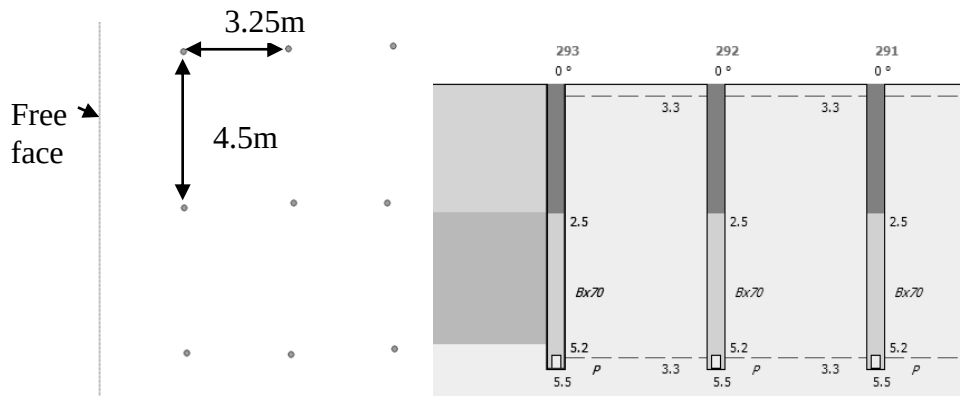

Figure 7. Hole pattern and loading plan for a standard blast.

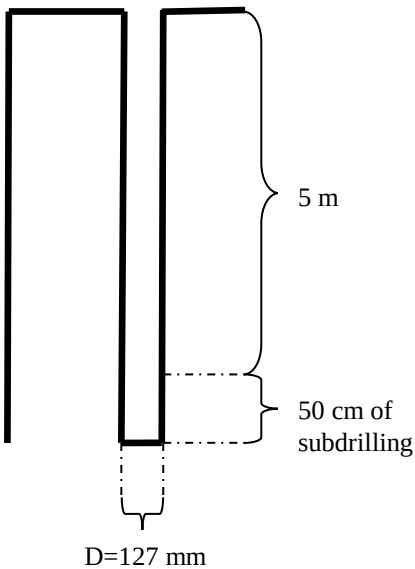

Figure 8. Drill pattern used for a standard blast.

a qualitative way from muckpile photos and excavating operator's feedback.

2 FIELD TESTS CONDUCTED

This study is mainly focused on the influence of stemming and initiation sequence on the blast. Consequently we have acted on these parameters. The explosives used are the same in all the following blasts. In order to establish a reference basis of results to compare our tests with, we first monitored several blasts without changing any parameters. For this paper we will term them as 'standard blasts' (Figures 7, 8 and 9), are characterised by a delay of 0 ms between holes of a same row, and a stemming of 2.5 m. The delay between two rows is 42 ms and will never change in the study. Then, we conducted one test with a 2.7 m stemming and a standard sequence, three tests with a 9 ms delay between holes of the same row and a standard stemming, and one test with a stemming adapted for each hole to the rock fragmentation measured by rigs.

Table 1. Summary table of recorded blasts with their initial settings.

Blast	Initial settings
110b3001	0 ms 2.5 m stemming
115b3001	0 ms 2.5 m stemming
110g3011	0 ms 2.5 m stemming
105g5007	0 ms 2.5 m stemming
110b3002	0 ms 2.5 m stemming
115b3002	0 ms 2.5 m stemming
110b5011	0 ms 2.5 m stemming
115g3011	0 ms 2.7 m stemming
110b3003	9 ms 2.5 m stemming
115b5010	9 ms 2.5 m stemming
110b5012	9 ms 2.5 m stemming
115b5009	9 ms adapted stemming 2.7/2.5/2.4 m

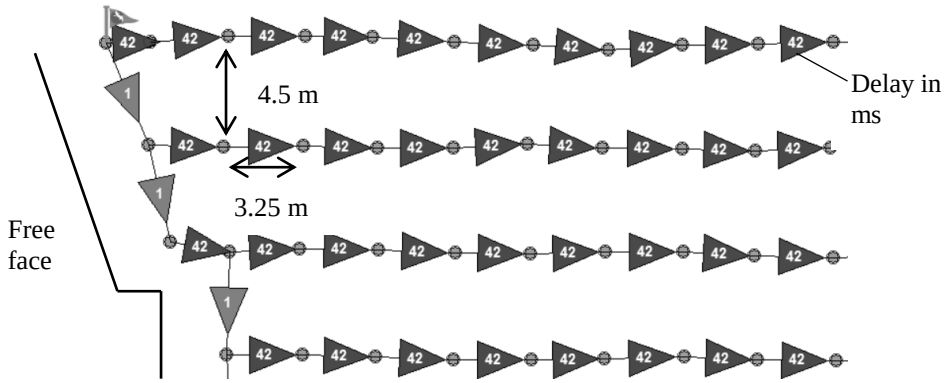

Figure 9. Sequence used in a standard blast (Nonel sequence).

A summary of all monitored blast is presented in Table 1.

3 RESULTS

3.1 Effect of initiation sequence on the direction of movement

As presented in Figure 10, the superposition of ore polygons and isochrone lines calculated in Expertir from the initiation sequence, shows that the movement is perpendicular to isochrones. We found the same result for all the monitored blasts independently of initials parameters used in blasts.

3.2 Effect of the 2.7 m stemming

It's important to note that both blasts presented in

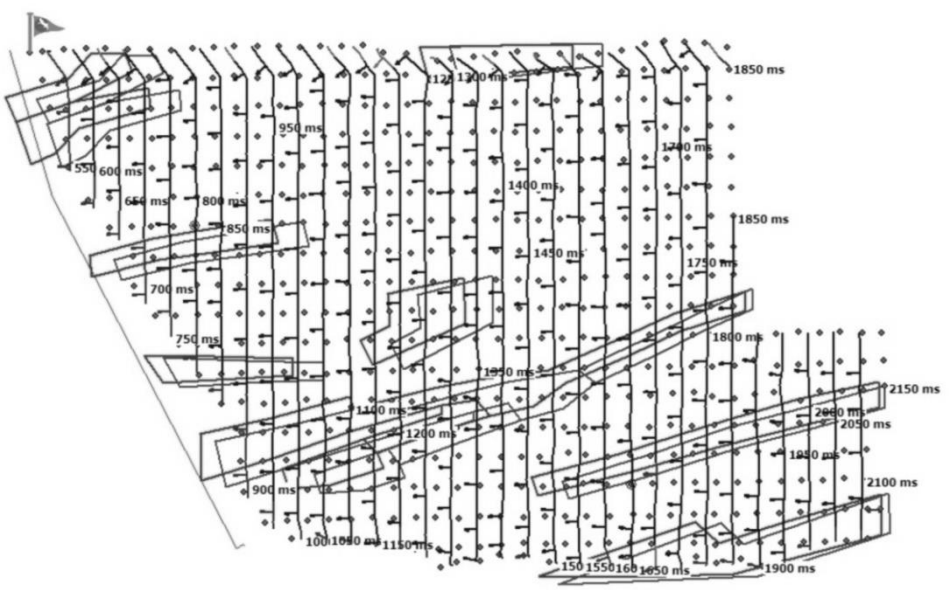

Figure 10. Correlation between ore movement (initial position, with final position moving to the left) and isochrones (vertical lines).

Table 2 were shot one above the other. Blast 110g3011 is situated on the level -105 m in the open pit; blast 115g3011 is situated on the level -110 m. The number 3011 is the reference of their position. Consequently, we can make the approximation that the rock is the same for both blasts; the only parameter to have changed is the stemming height.

Table 2. Summary table of recorded swellings.

	Avg Swelling(cm)	Swelling StdDev(cm)
115g3011 (2.7 m stemming)	207	67
110g3011 (2.5 m = standard)	140	79

Even if there are no BMM® sensors in this blast, the video shows us a better movement. In this blast, there is much less flyrock. According to the excavating operator's feedback, the bottom and middle layers are easier to dig than in a standard blast. But the top layer contains a lot of big rocks which is bad for the dilution.

The longer stemming leads here to two phenomena:

- the better gas retention creates a higher swelling and a finer fragmentation for both middle and bottom layers even if there's less energy in the hole since the stemming is longer
- this more important stemming means that there is less energy at the top of the column which leads to the coarser fragmentation on the top layer of the muckpile

3.3 Effect of the 9 ms delay

Except for the isochrones orientation, there isn't any noticeable quantitative differences of swelling and horizontal movement between blasts with 9 ms delay and standard blasts recorded (Figures 12 and 13).

The feed-back from excavator operators reveals that it is easier to dig in muckpiles from a 9 ms blast. The tiny delay of 9 ms between the holes creates more open faces when a hole is going to explode (Hustrulid 1999) Consequently, there is more shock energy efficiently used for cracking the rock. This explains the better fragmentation obtained with this delay. The fragmentation has only been evaluated qualitatively with feedbacks from excavating operators.

Figure 11. Coarse fragmentation at the top of the muckpile from blast 115g3011 with 2.7 m stemming.

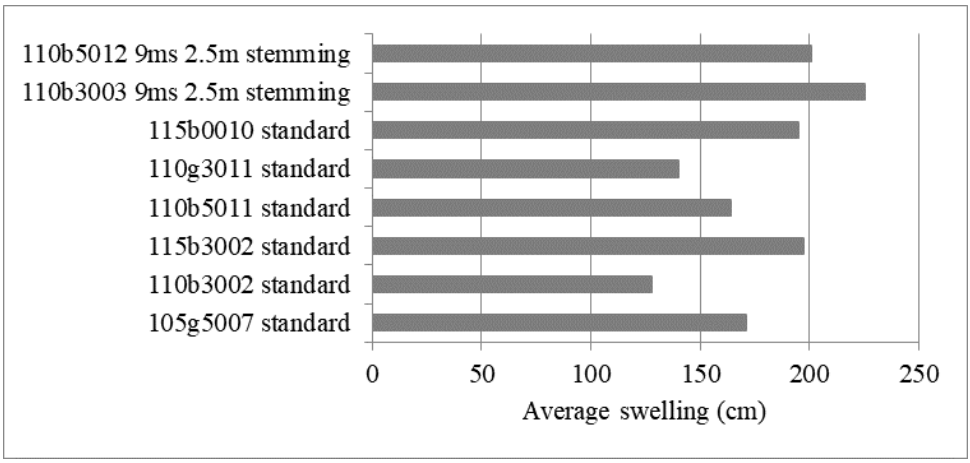

Figure 12. Average swelling recorded from swelling fields.

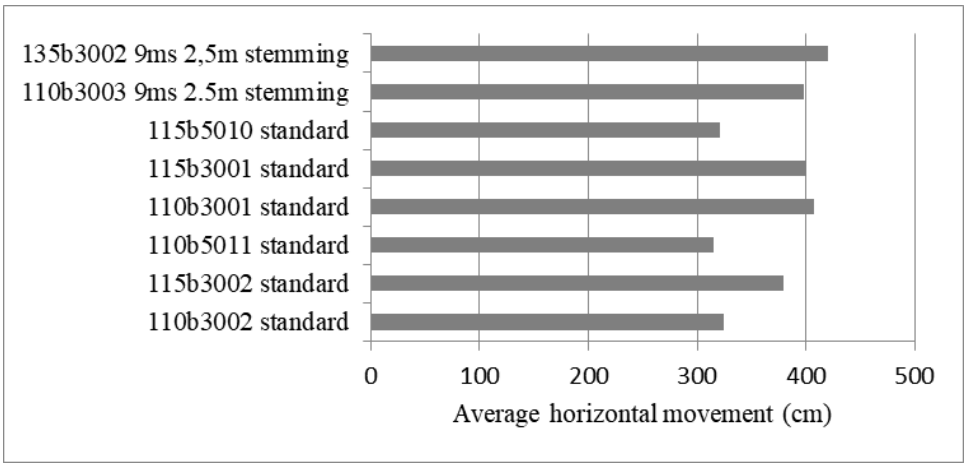

Figure 13. Average horizontal movement recorded with BMM® sensors.

3.4 Effect of stemming blown out and cracks on the muckpile shape

Each blast is filmed. On blasting videos, we can see several stemming columns blow out. We can also observe areas with smaller swelling where a blow-out happened. A photo taken of those areas also shows a coarser fragmentation in the muckpile's first layer (Figures 14, 15).

Stemming columns blown out aren't the only explanation for areas with smaller swelling. As shown in the following figures, the existence of open cracks or fractures has an impact on the rock movement.

Unlike in a blow-out area, there is no coarse fragmentation observed on the area with small swelling in this case.

We observe here two negative phenomena for the dilution:

– blow-outs because they create a coarse fragmentation and flyrock projections
– the variation in material movements from one point to another because they create a rock mixing

Both phenomena are correlated with a smaller local swelling. Therefore, we will get a lower

Figure 14. Blast 110b5011: correlation between stemming blow outs and smaller swelling.

Figure 15. Blast 110b5011: coarse fragmentation at the blow out location.

dilution from a muckpile with a smaller standard deviation of the swelling when average swelling is acceptable.

3.5 Effect of the varying stemming lengths on the movement

For this test, stemming values were increased from 2.5 m to 3 m according to the surface fracturing of the rock as measured by the drilling rigs (Hustrulid 1999). We used the penetration rate information in Expertir to calculate an optimal stemming length for each hole (Figures 18, 19).

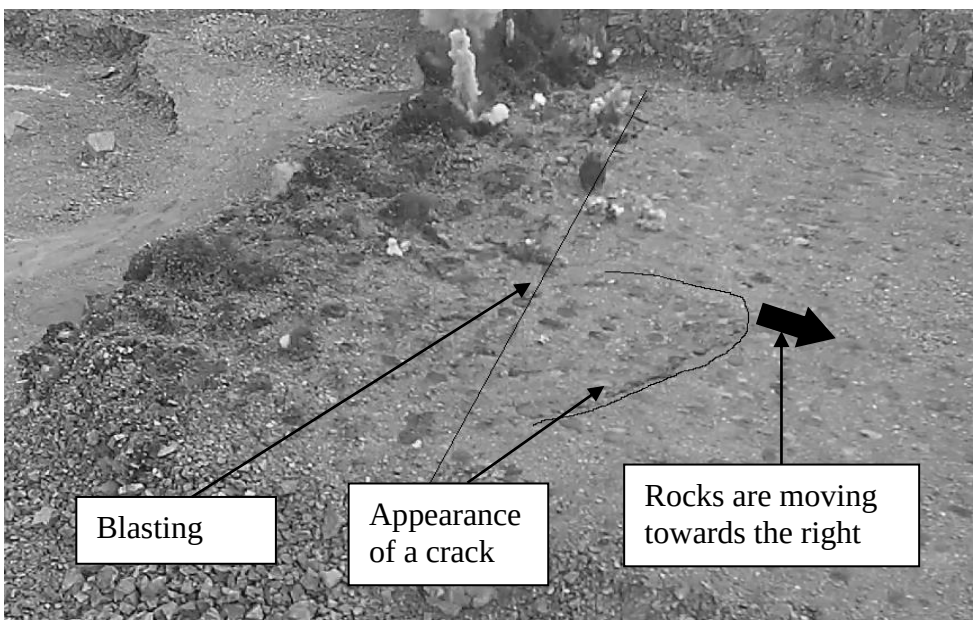

Figure 16. Blast 110b5012: effect on a crack in the rock mass seen on the video.

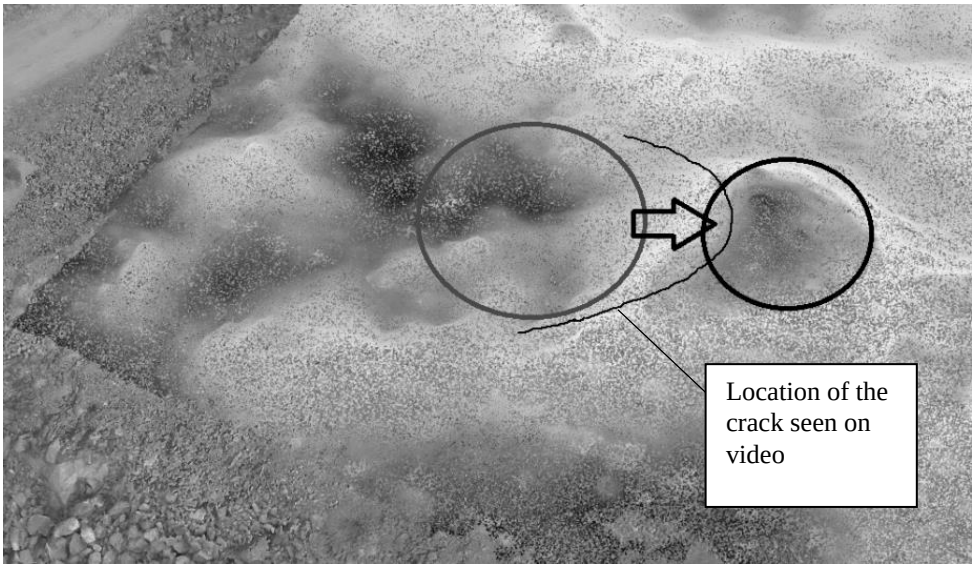

Figure 17. Blast 110b5012: effect on a crack seen on the swelling field.

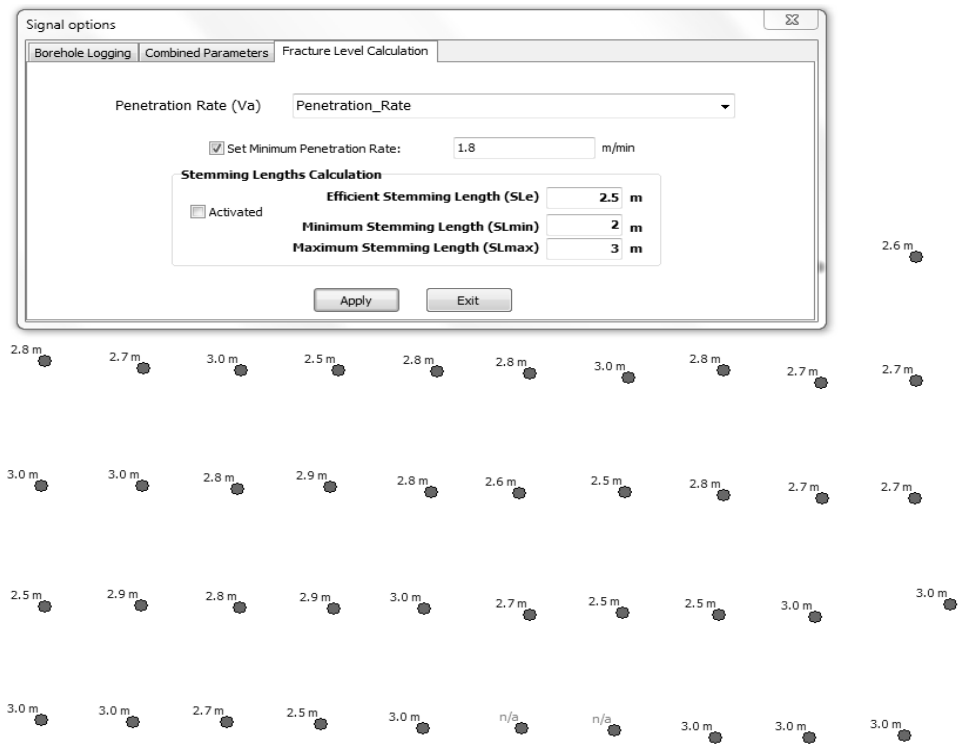

Figure 18. Different stemming lengths in the same blast, calculated by Expertir.

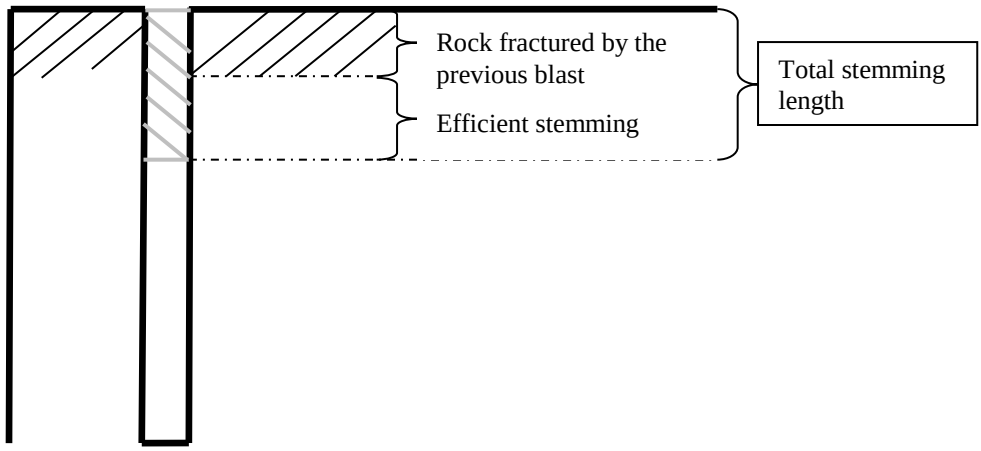

Figure 19. Definition of efficient and optimal stemming lengths.

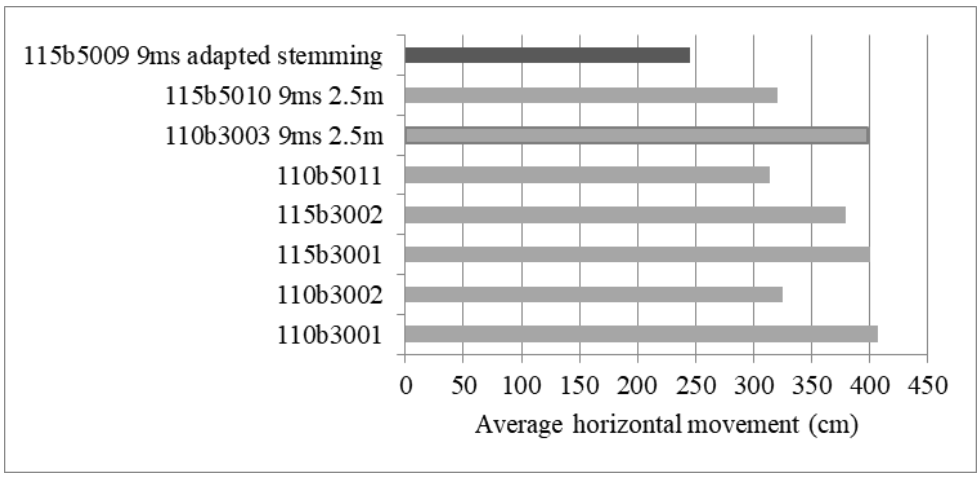

Figure 20. Horizontal movement comparison for different initials parameters.

The optimal stemming length is calculated in the following way: as shown in Figure 18, it is possible to set in Expertir an efficient stemming length (here it is 2.5 m). The depth of rock fractured by the previous blast is then taken into account, if for example 30 cm of fractured rock is measured by the rig, then 2.8 m of total stemming will be displayed in Expertir. In order to avoid putting too much stemming in a hole, a maximum stemming length is set (here 3 m).

The results for the horizontal movement measured with BMM® sensors are presented in Figure 20.

We can see here a noticeable decrease in the horizontal movement of the blast with a differential stemming. There isn't any major difference concerning other measured parameters. The feedback from excavating operators told that the muckpile wasn't harder to dig than usual.

4 DISCUSSION ON DILUTION AND CONCLUSION

We have seen that a stemming blow out was correlated with a smaller local swelling and a coarser fragmentation. Coarser fragmentation in

the muckpile leads to more dilution, the flyrock projected by the blow outs also leads to more dilution. Furthermore, if the muckpile swelling is not even, there's a larger chance to have some rocks moving from the highest parts of the muckpile to the lower parts which also leads to more dilution. Consequently, it is important to limit as much as possible stemming blow outs. When we used varying stemming lengths, we also observed an overall smaller horizontal movement, which is also a good point for reducing the dilution. In mines characterised by a heterogeneous fragmentation of the top layer, using a varying stemming length can be a good way to achieve the goal of reducing stemming blow outs and dilution.

The mapping of swelling fields appeared to be a very effective way for evaluating quantitatively the shape of a muckpile. An ideal blast should lead to a homogeneous and vertical swelling: the vertical standard deviation of a muckpile should ideally tend to 0. The swelling should be important enough for allowing an easy digging: this condition is measurable by the means of the swelling for the whole muckpile. Both the mean and standard deviation values for a muckpile are easily measurable from the swelling field.

Finally, it is important to keep a critical eye on the job done here: the correlation between stemming blow outs, small swelling and coarse fragmentation has been observed in many cases and can be believed to be valid. However it is not the case for the smaller horizontal movement observed on the blast with varying stemming. Even if the movement reduction was clear compared to all other monitored blasts; it is important to confirm the result we got there by testing the varying stemming on at least one more blast since blasting involves a lot of unexpected and more or less random effects.

REFERENCES

Hustrulid, W. 1999. *Blasting principles for open pit mining*, Volume 1, *General Design Concepts.* A.A. Balkema, Rotterdam, 382p.Chapter 4.9, *Measure-while-drilling system*, p. 101-106; Chapter 5.6, *Some sequencing principles*, p. 144-149.